The Dissertation (or Treatise) Committee for Maruthi Nagavalli Yogeesh Certifies that this is the approved version of the following dissertation (or treatise):

Flexible High Frequency Electronics and Plasmonics using Two Dimensional Nanomaterials

Committee:

Deji Akinwande, Supervisor

Sanjay Banerjee

Ananth Dodabalapur

Yuebing Zheng

Keji Lai

Flexible High Frequency Electronics and Plasmonics using Two Dimensional Nanomaterials

by

Maruthi Nagavalli Yogeesh, M.S

Dissertation

Presented to the Faculty of the Graduate School of

The University of Texas at Austin

in Partial Fulfillment

of the Requirements

for the Degree of

Doctor of Philosophy

The University of Texas at Austin

December 2017

Dedication

This is dedicated to the lord for his endless love and support

Acknowledgements

First, I would like to sincerely thank my Ph.D. adviser, Prof. Deji Akinwande for giving me the wonderful opportunity to work in his research group. I am very fortunate to work on projects related to flexible electronics and plasmonics. He is a role model to young researchers like me. He built in me skills needed to become a real scientist, entrepreneur and good teacher.

I am grateful to Prof. Sanjay Banerjee for his guidance and support on many different projects related to 2D electronics. I would like to appreciate help received from his group members – Hema Mowa, Amritesh Rai, Atresh Sanne, Dr. Rudresh Ghosh and Dr. Sushant Sonde. They were always ready to help with any issues related device fabrication or measurements.

I am also grateful to Prof. Yuebing Zheng for his guidance and support on projects related to 2D plasmonics. I also like to appreciate support of his group members –Dr. Linhan Lin and Zilong Wu. We worked on couple of projects like one team. I will always remember the late night meetings with them at MER.

I am grateful to Prof. Dodabalapur and his group members - Barrett, Seohee and Bongjun. I learnt many interesting facts on organic and printed electronics from them.

I want to sincerely thank Prof. Lai and his group member – Dr. Di Wu. I will always remember the research meetings with Di on MIM measurements and metal contacts for FETs.

I would also like to appreciate support from my group members Dr. Kristen Parish, Dr. Jongho Lee, Dr. Li, Dr. Sherry Chang, Dr. Fahad Chowdary, Weinan Zhu, Wei Li and Saungeun Park.

Finally, I would like to thank my family members for their generous support and unconditional love. None of this would have been achieved without them.

Flexible High Frequency Electronics and Plasmonics using Two Dimensional Nanomaterials

Maruthi Nagavalli Yogeesh, Ph.D.

The University of Texas at Austin, 2017

Supervisor: Deji Akinwande

In this work, we have demonstrated novel flexible electronics and plasmonic devices using 2-dimensional (2D) nanomaterials (graphene and MoS_2). The first part of this work is about design of flexible high frequency electronics using 2D nanomaterials. We report sub-THz graphene transistors with f_T ~ 100GHz. We also discuss how to integrate graphene based sub blocks (antenna, mixer and speaker) to fabricate all graphene based wireless receiver. We report for the first time flexible RF transistors with GHz frequency response using CVD grown monolayer MoS_2. We also demonstrate flexible low power RF nanosystems (amplifiers, mixers, AM receiver) using CVD MoS_2. We have developed MoS_2 transistor models for integrated circuit design application. RF MoS_2 transistors results are very promising for low power internet of things (IOT) applications. In second part, we have shown design of novel plasmonic devices using 2D nanomaterials. We have demonstrated large area tunable graphene metasurface using moiré nanosphere lithography (MNSL). We have shown novel method to fabricate large area graphene nanoribbons (GNRs) using block copolymer lithography (BCPL) and its potential application towards tunable mid-IR plasmonic sensing. We report for the first

time nanopatterning of CVD MoS_2 on plasmonic substrate using bubble pen lithography (BPL). We have also shown light enhancement of monolayer CVD MoS_2 using plasmonic nanoantenna array (PNA). These results are very useful for design of highly efficient 2D nanomaterial based LEDs, photodetectors, lasers and sensors.

Table of Contents

List of Tables

List of Figures

PART1: *FLEXIBLE HIGH FREQUENCY ELECTRONICS USING 2D NANOMATERIALS*

Chapter 1: 2D Nanomaterials based Flexible Electronics

Flexible electronics is currently one of the fastest growing research area. Fig 1.1 illustrates some of the next generation flexible smart systems – smart phones, wearable sensors, smart tablets and more [1]. Lots of effort is being put in developing new materials for flexible smart systems [1-4] . These materials should have good electrical, optical and mechanical properties. In the following chapters, we will be showing why two dimensional (2D) nanomaterials (Fig 1.2) like graphene and transition metal dichalcogenides (TMDs) -MoS_2 are promising candidates for flexible high frequency electronics [1-7].

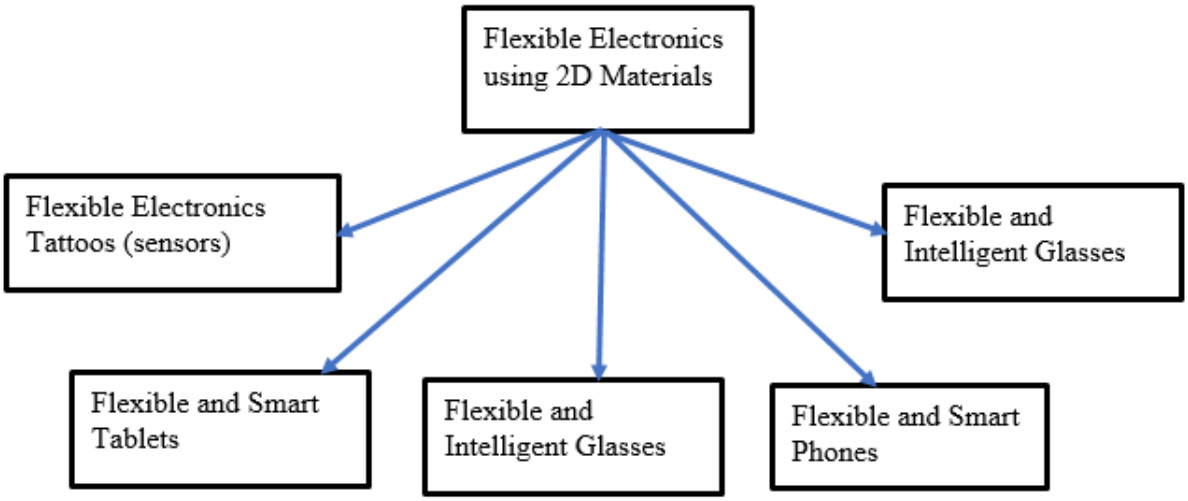

Figure 1.1. Illustration of flexible smart systems (smart watches, sensors, glasses, cellphones). Adapted from [1]

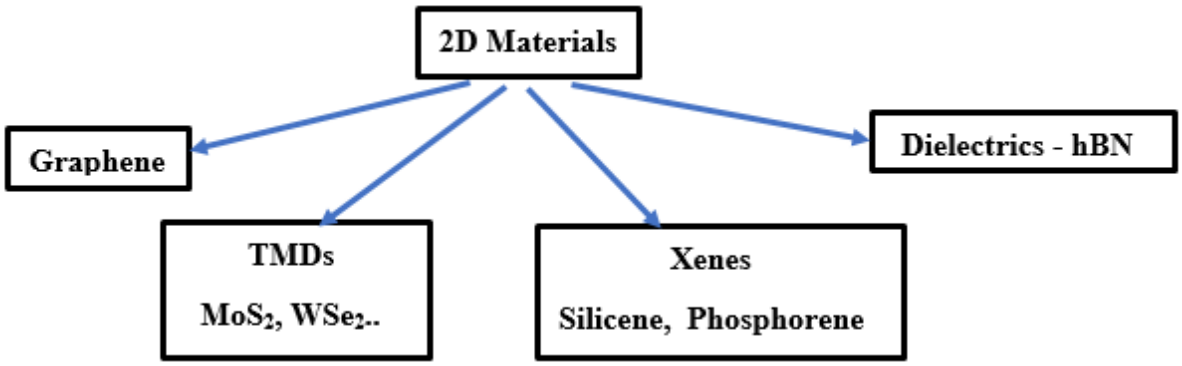

Figure 1.2. Three-dimensional illustration of 2D monolayers. Adapted from [1]

In chapter 2, we discuss in detail design of high frequency flexible RF electronics using graphene. We demonstrate record RF performance using graphene based transistors with f_T ~ 100GHz. These results are very interesting for flexible millimeter wave or sub THz nanosystems.

In chapter 3, we discuss the design of flexible RF electronics using CVD monolayer MoS_2. We demonstrate for the first-time flexible MoS_2 RF transistors with f_T ~ 5.6GHz, f_{MAX} ~ 3.3GHz. Along with flexible MoS_2 RF transistors, we have also demonstrated top gate MoS_2 RF transistors on Si substrate with f_T ~ 6.7GHz, f_{MAX} ~ 5.3GHz and embedded gate MoS_2 transistor with record f_T ~ 20GHz, f_{MAX} ~ 11.4GHz. We also designed and measured flexible RF circuits (amplifiers, mixer and AM demodulators) using MoS_2 transistors. Finally, we have developed a simple RF models to help with design of future MoS_2 based integrated circuits. These results are very

promising for design of flexible low frequency and low power internet of things (IoT) applications.

Chapter 2: Flexible Electronics using Graphene

INTRODUCTION

Graphene is a 2D nanomaterial with high room temperature mobility (> 1000cm^2/V.s), good electrical and thermal conductivity, and good mechanical strength (strain limit ~ 20%). This makes it an ideal candidate for high frequency flexible electronics [8]. Some important research works includes demonstration of graphene based integrated circuits compatible with Si fabrication [9]and also graphene based flexible circuits [10]. In this work, we demonstrate graphene based flexible RF transistors with record f_T ~ 100GHz and also present design of basic building blocks (antenna, demodulator, and speaker) of an all graphene based radio receiver.

FLEXIBLE GFET FABRICATION AND CHARACTERIZATION

We fabricated embedded gate graphene transistor with channel length lg ~ 250nm and width w~ 60um (6 fingers of 10um width). Gate fingers (Ti/Pd - 2nm/40nm) and gate dielectric (ALD AL_20_3 ~ 10nm thick) are first deposited on cured flexible polyimide substrate. CVD grown graphene is transferred onto this substrate. Top drain and source contacts (Ti/Au – 2nm/50nm) is patterned using EBL [8]. Fig 2.1a shows the 3D illustration of graphene transistors and Fig 2.1b shows the enlarged optical image of the graphene transistor. We carried out room temperature electrical measurement of the graphene transistor. Fig 2.1c, d shows the input and output characteristics of graphene transistor. Our best device showed electron mobility 9050 cm^2/V·s and hole mobility ~ 3000 cm^2/V·s. We attribute these high values of mobility and current saturation due to high quality of graphene, smooth PI substrate and good ALD dielectric.

Note: This chapter results are published in the journal - *M. Yogeesh, et.al; Towards the Realization of Graphene Based Flexible Radio Frequency Receiver. Electronics* ***2015,*** *4.* I am first author and contributed for many experiments presented on this journal.

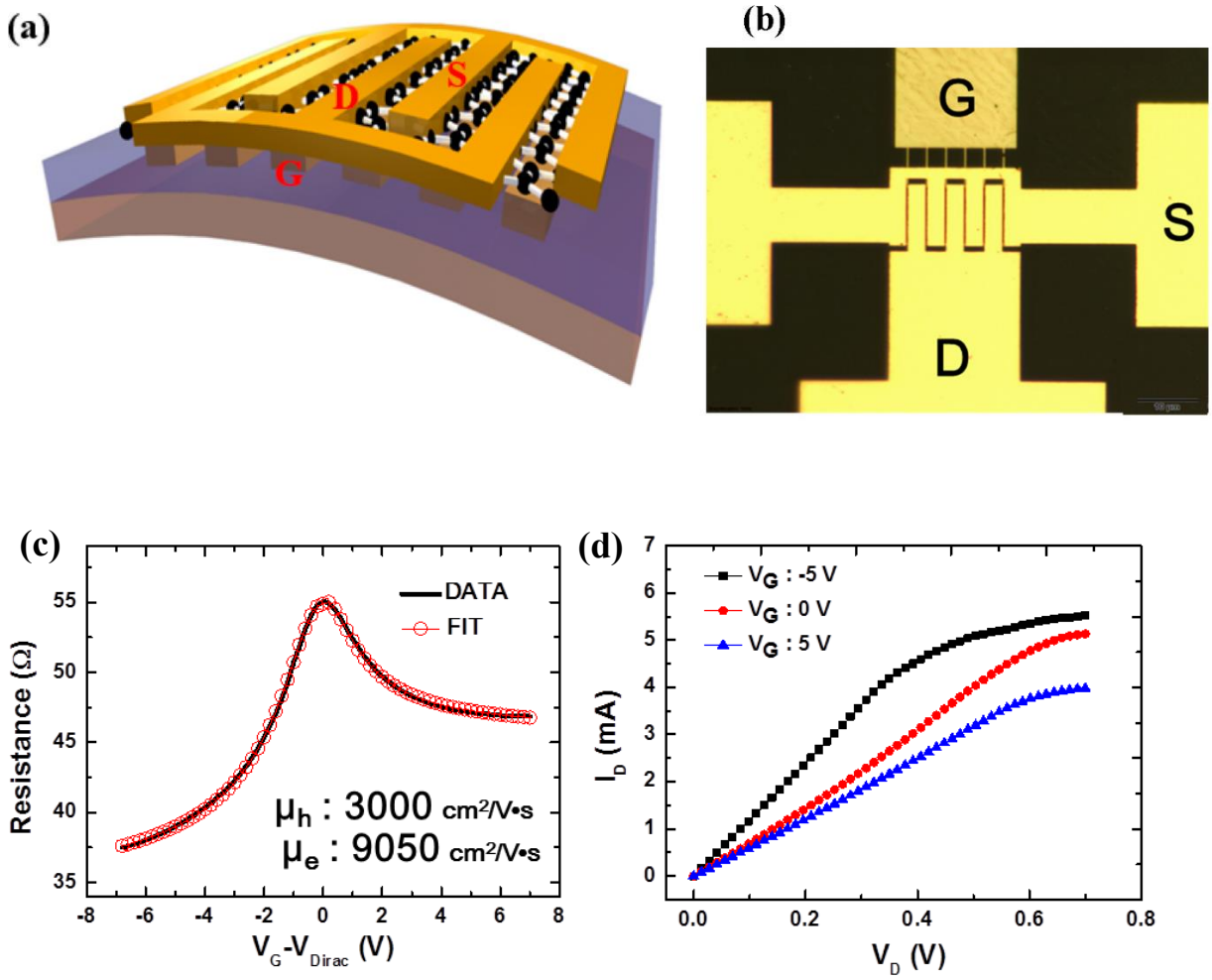

Figure 2.1. (**a**) 3D illustration of graphene transistor on flexible polyimide film; (**b**) Enlarged optical image graphene transistor. (c) Input characteristics of graphene transistor (V_D = 10 mV). (d) Output characteristics (I_D - V_D).

FLEXIBLE GRAPHENE TRANSISTOR RF PERFORMANCE

We did RF measurement of graphene transistor. The procedure is mentioned in more detail [8]. RF performance is often described by frequency (f_T) at which current gain (h_{21}) becomes unity and also the frequency (f_{MAX}) at which power gain (U) becomes unity. Equation 1 and 2 shows the dependence of f_T and f_{MAX} on transistor parameters (transconductance g_m, gate capacitance C_{gs}, parasitic gate-drain capacitance $C_{p,gs}$, parasitic gate-source capacitance $C_{p\text{-}gd}$ and gate resistance R_g). Fig 2.2a shows the current gain h_{21} of the graphene transistor on flexible polyimide substrate. We obtained intrinsic f_T ~18 GHz and f_{MAX} ~ 2.1GHz. We also did measurement of graphene transistor fabricated on willow glass substrate and it showed a record performance with f_T ~ 100GHz (see Fig 2.2b). We attribute this to high thermal conductivity of willow glass compared to polyimide substrate [11-12].

f_T can be further improved by reducing channel length and design of better layouts (reduced parasitics). f_{MAX} is lower for flexible devices compared to devices fabricated on rigid Si substrate mainly due to poor thermal dissipation of flexible polymer substrate. These GFETs cannot handle high drain bias (V_D > 0.5V). Thermal breakdown takes place when operated at high bias [1, 5]. f_{MAX} can be further improved by using good thermal conducting films on flexible substrates.

$$f_T = \frac{g_m}{2\pi(C_{gs}+C_{p,gs}+C_{p,gd})\left((R_{p,s}+R_{p,d})g_d+1\right)+C_{p,gd}g_m(R_{p,s}+R_{p,d})} \quad \text{---------[1]}$$

$$f_{MAX} = \frac{f_T}{\sqrt{2g_d(R_{p,s}+R_{gate})+2\pi f_T C_{p,gd}R_{gate}}} \quad \text{-------- [2]}$$

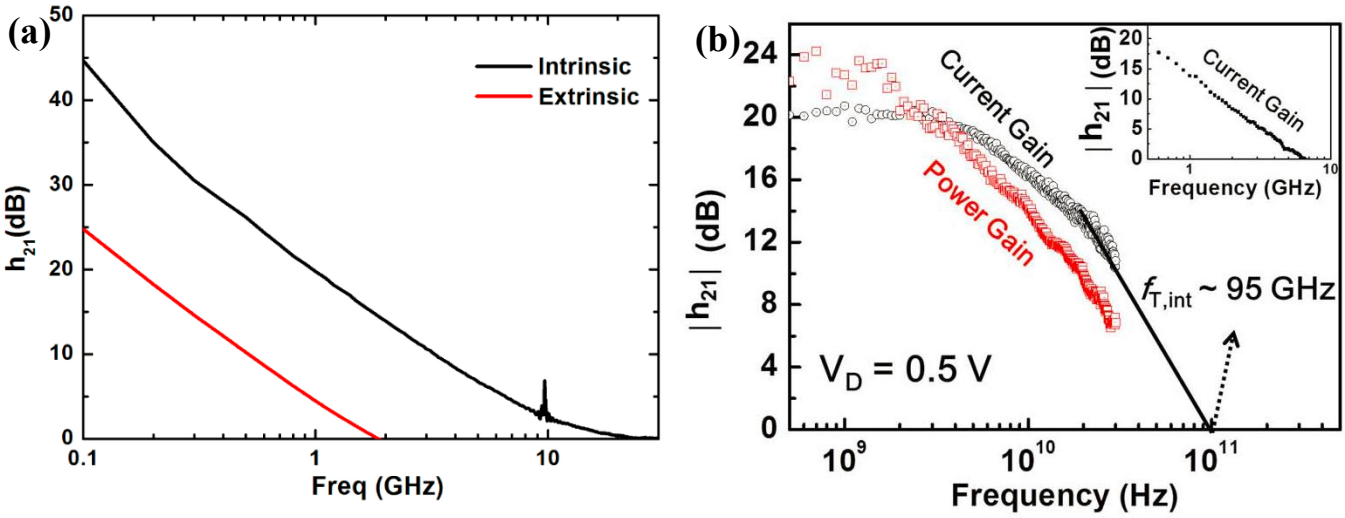

Figure 2.2. (a) Current Gain (h_{21}) of graphene transistor with (a) f_T ~18 GHz for graphene transistor on PI substrate. (b) f_T ~95GHz for graphene transistor on willow glass substrate. Reproduced from [8, 11-12]

GFET Flexibility and Reliability

Mechanical flexibility of GFET was measured using bending test fixtures [3, 5]. DC probes were landed on source, drain and gate contacts. The bending of the device was increased and simultaneously DC measurements were carried out. This process was carried out until device breakdown. The device can sustain maximum bending strain of 8.6%. The channel resistance and mobility remained above 80% of its flat value. Strains greater than 8.6% resulted in gate dielectric breakdown and increased gate leakage [5, 10].The reliability measurements of GFETs encapsulated with Si3N4 and Cytop was carried out (see Fig. 2.3). These devices were exposed to DI-water and other solvents to evaluate its performance. The device performance was above 80% of its initial performance even after 2 days of exposure.

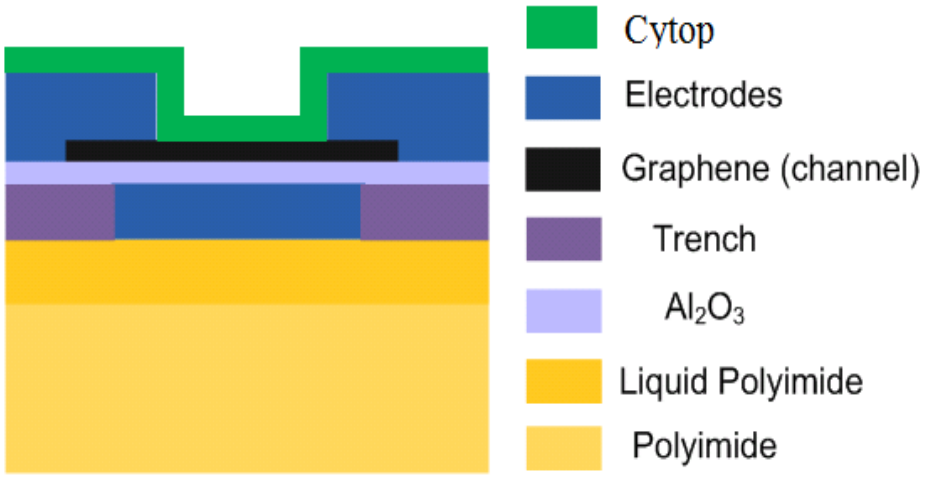

Figure. 2.3. GFET encapsulated with CYTOP

FLEXIBLE GRAPHENE TRANSISTOR BASED RF CIRCUITS

Fig 2.4 shows the block diagram of graphene based RF receiver. This receiver front end has a graphene (or graphite) based microstrip patch antenna, followed by graphene based demodulator, whose output is connected to graphene speaker. In this section, we will showing working principle of graphite based microstrip patch antenna, graphene based demodulator and speaker. Readers can refer to our work [8] on more details about design of flexible graphene receiver.

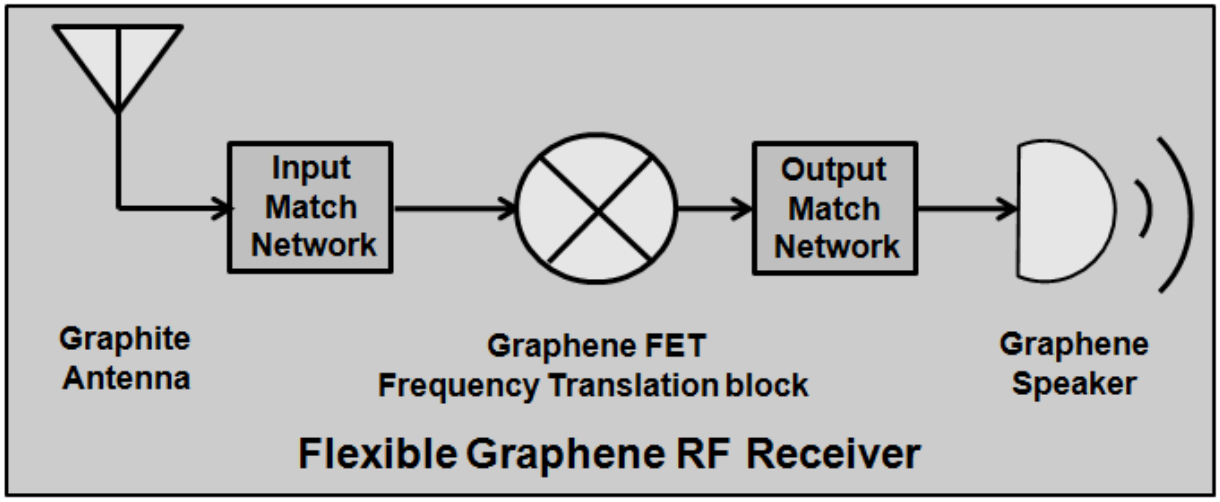

Figure 2.4. Block diagram of graphene based RF receiver.

Graphene Based Flexible Antenna

We designed and fabricated graphite based microstrip patch antennas at 2.4GHz on flexible polyimide substrate [8, 13-15]. The performance of this antenna is very close to copper based patch antenna. This antenna is designed towards the goal of achieving an all graphene/carbon flexible RF receiver system. The antenna was designed using a graphite sheet since it is more conductive than monolayer graphene at microwave frequencies. Graphite sheets have very good flexibility and thermal conductivity compared to copper. Antennas can be easily fabricated using graphite sheets on a roll to roll facility when

compared to copper based antennas. We can also tune DC conductivity of intercalated graphite antennas. This can be used for design of sensors and reconfigurable RF systems. This patch antenna fabricated on a polyimide substrate is shown in Fig. 2.5a. The antenna simulation results from using a 3D electromagnetic solver, (CST) and measurement results are shown in Fig. 2.5b. The antenna dimensions are width w = 39.11mm and length L= 30.95mm. Far field radiation pattern is shown in Fig. 2.5c.

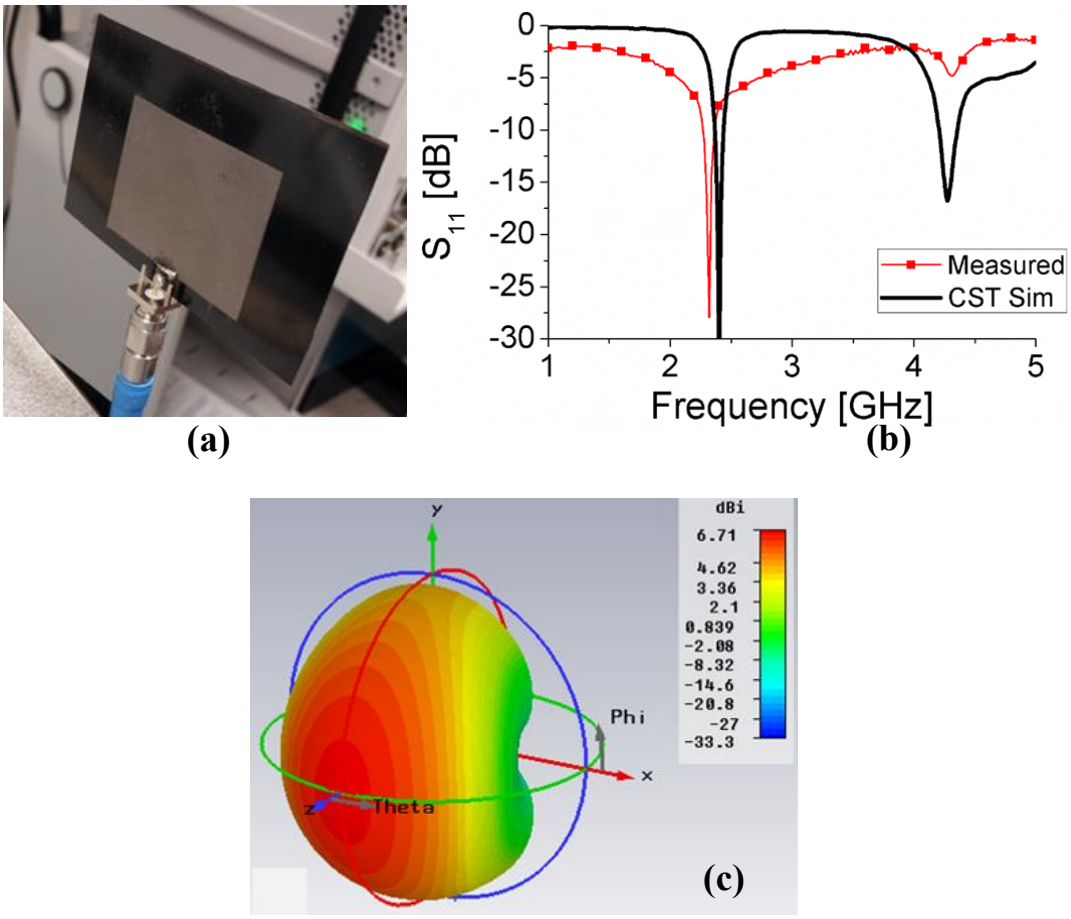

Figure 2.5: (a) Graphite Patch Antenna. (b) Measured and simulated response (c) Simulated far field radiation pattern

To observe the flexibility of the antenna, convex bending tests were carried out as shown in Fig. 2.6a. The antenna was placed in the middle of a test vice fixture and slowly bent (see Fig. 2.6b). The S_{11} was measured for each 1mm bending radius (see Fig. 2.6c). The resonant frequency changes are very small down to 30mm bending radius. The reason for getting broader S11 during bending tests (Fig. 2.6c) should be due to poor input SMA connection of the antenna used for bending tests. This result offers new opportunity for all carbon/graphene RF electronics that can be integrated with flexible substrates, including bendable GHz electronics and antennas.

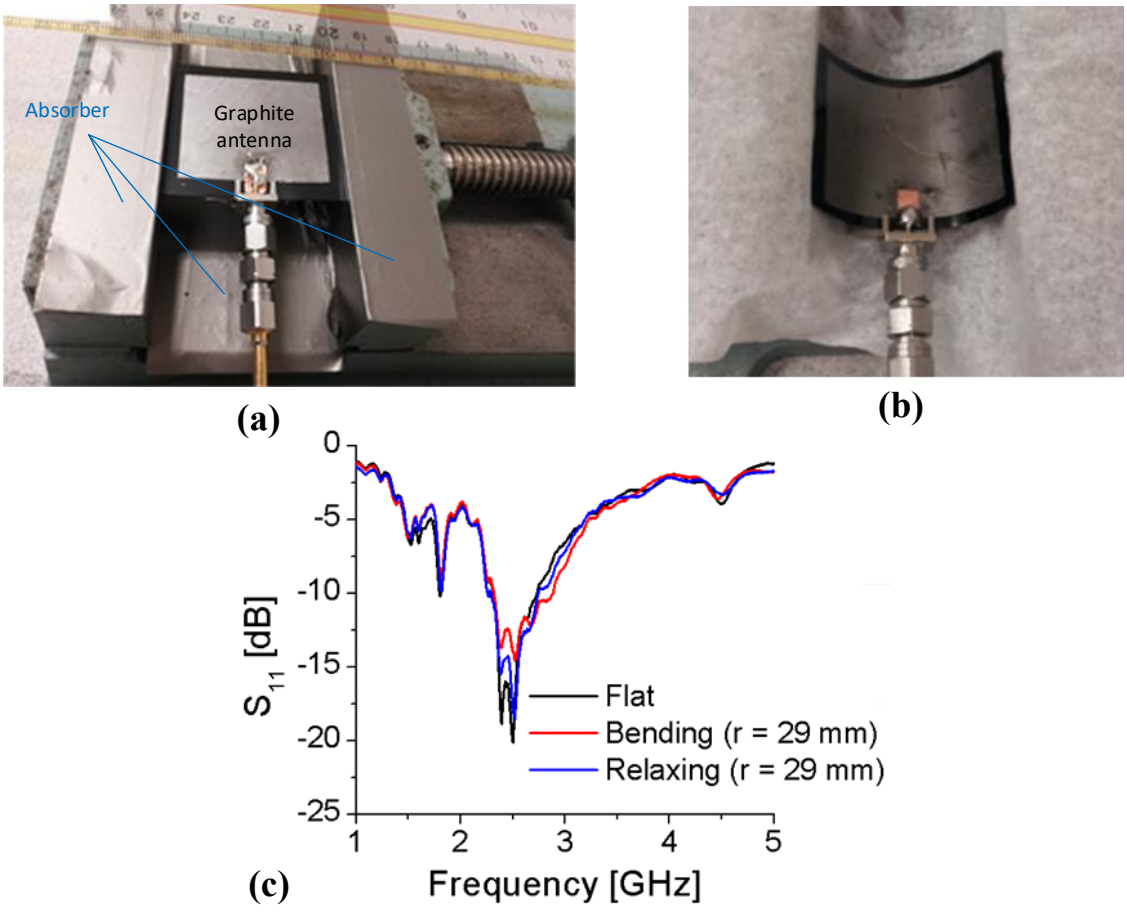

Figure 2.6: (a) Convex bending of graphite antenna. (b) Antenna is placed in the middle of test vice fixture. (c) Antenna response with convex bending of r=29mm.

Flexible Graphene Transistor based AM demodulator

Fig 2.7a shows the schematic of graphene transistor based amplitude modulation (AM) demodulator. We operate graphene transistor near dirac point. The ambipolar characteristics of graphene input characteristics makes it act like a square law detector [10, 14-15]. This principle is used for demodulation. We applied an AM input signal (modulating signal @ 2KHz, Carrier @ 400MHz) to gate of transistor. Demodulated output at drain contact is low pass filtered (using smoothening capacitor Cc) and observed on oscilloscope. Gain of our demodulator is ~ -34Db (see Fig 2.7b,c). The output is noisy due to poor low pass filter. The gain performance is on the low end for the current devices due to parasitics from the source and drain contacts and interconnects. This circuit can be modified and used for different modulations – Amplitude shift keying (ASK), phase shift keying (PSK) and frequency shift keying (FSK) [16].

(a)

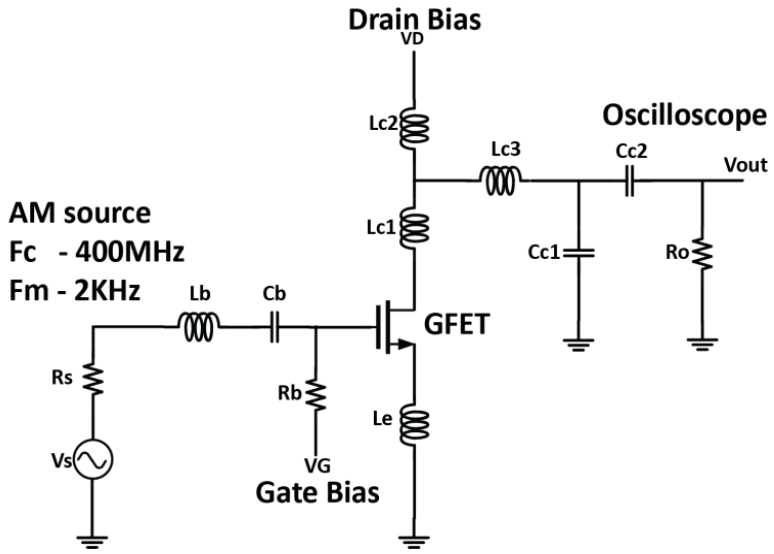
Drain Bias
VD
Lc2
Oscilloscope
Lc3
Cc2
Vout
AM source
Fc - 400MHz
Fm - 2KHz
Lc1
Cc1
Ro
Lb
Cb
GFET
Rs
Rb
Le
Vs
VG
Gate Bias

(b)

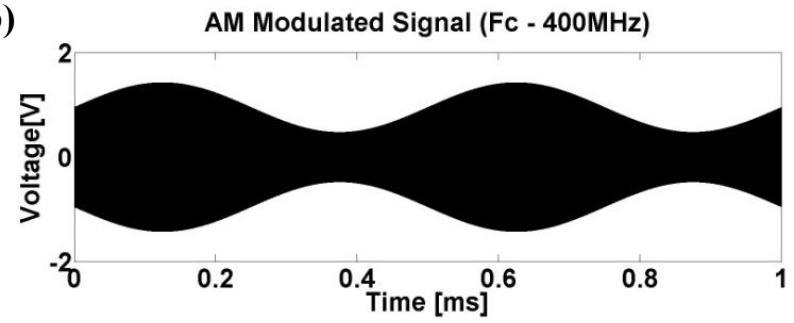
AM Modulated Signal (Fc - 400MHz)
Voltage[V]
2
0
-2
0
0.2
0.4
0.6
0.8
1
Time [ms]

(c)

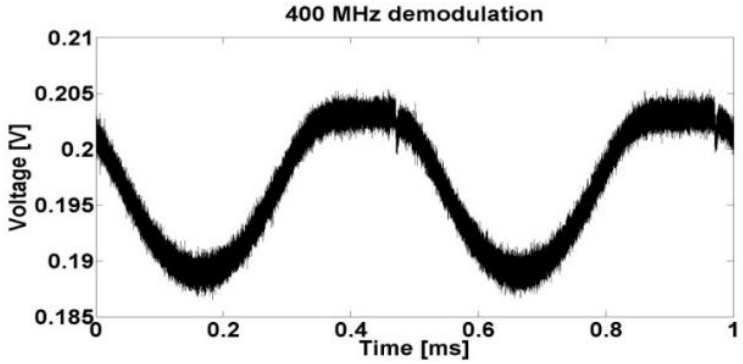
400 MHz demodulation
Voltage [V]
0.21
0.205
0.2
0.195
0.19
0.185
0
0.2
0.4
0.6
0.8
1
Time [ms]

Figure 2.7. (**a**) Flexible graphene transistor based AM Demodulator (**b**) AM input (mod signal ~ 2KHz, carrier @ 400MHz) and (**c**) Demodulated output. Reproduced from [8]

Flexible Graphene Speaker

Graphene has very good thermo-acoustic characteristics. It has very small heat capacity per unit area. This makes it an excellent material for thermo acoustic speakers. Tian et.al [17] demonstrated graphene speaker on paper substrate. Here, we demonstrate graphene speaker on PI substrate. Fig 2.8a shows the schematic of graphene speaker. CVD graphene is transferred onto flexible PI substrate. Two metal contacts (silver ink) are patterned at the edge of graphene film. We applied demodulated electrical signal between the two contacts. This signal will generate thermal oscillations at graphene – air interface. These oscillations are converted to audio/sound waves. Microphone is placed at a distance of 3cm to measure audible signal. Fig. 2.8b shows the microphone setup to measure sound power. Fig 2.8c shows the sound pressure level (SPL) of our speaker in comparison with Al foil based commercial speaker. Interested readers can refer to our work [8] for more details about graphene speaker.

The speaker power at high frequencies is given by equation 6. It mainly depends on frequency of sound (f), heat capacity of air (γ), velocity of sound in air (v_g) thermal effusively of PI substrate (e_s) and air (e_a)[8, 17].

$$\boldsymbol{P_{speaker} = \frac{Ro}{\sqrt{2}r_o}\frac{\gamma - 1}{v_g}\frac{e_g}{e_s + a_c + e_g}q_o} \quad \text{------(6)}$$

We plan to integrate this device with the AM radio receiver. The performance of this speaker at low frequency can be improved by high quality graphene film, waveguide design and fabrication of suspended graphene speakers.

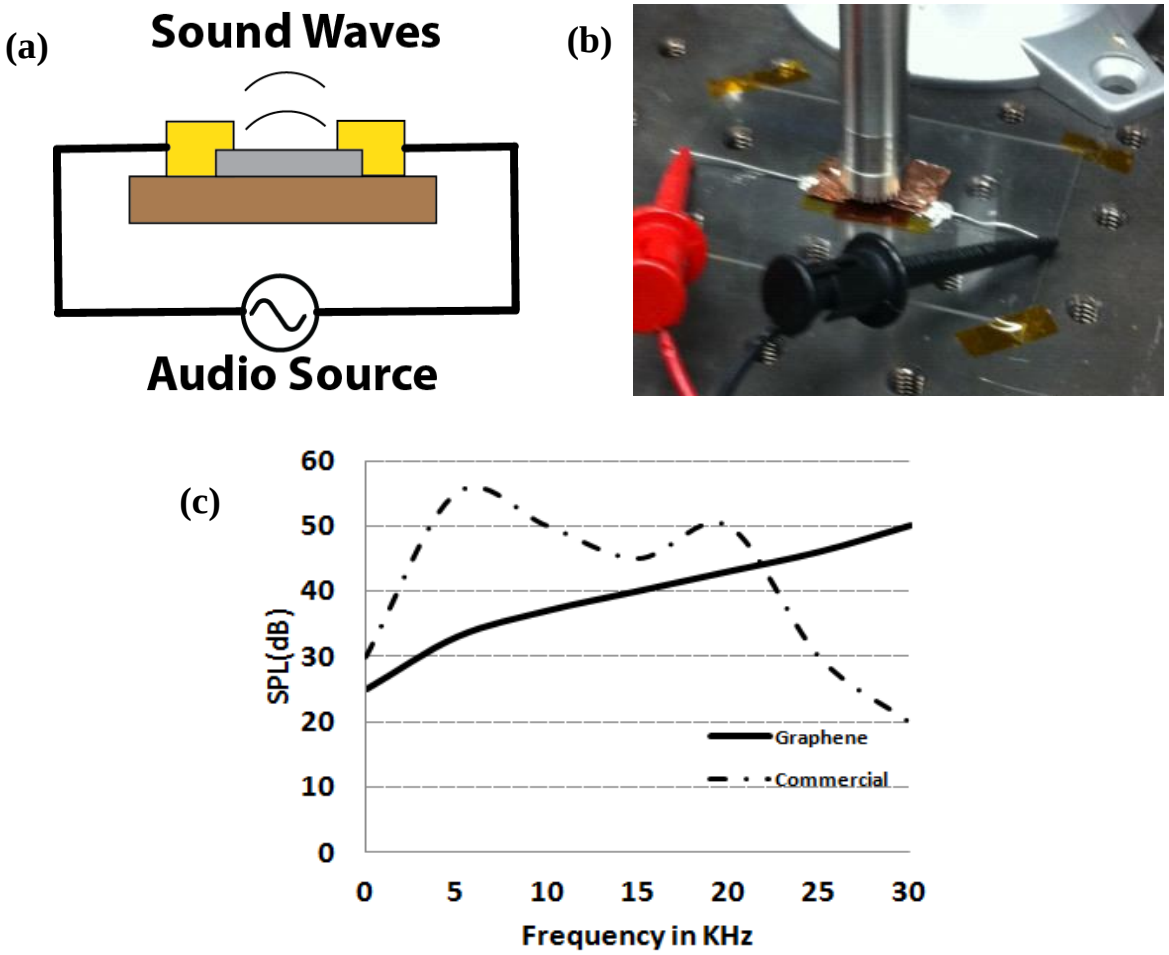

Figure 2.8. (**a**) Schematic of graphene speaker (grey—graphene, yellow—gold contacts, brown—flexible PI substrate); (**b**) graphene speaker measurement setup; (**c**) Sound pressure level (SPL) *vs.* frequency plot

Graphene AM Radio Receiver

The first graphene based flexible AM radio receiver at 2.4GHz was designed and fabricated. Fig. 2.9 shows the block diagram of the receiver. The receiver consists of a graphite antenna, GFET demodulator and speaker. The receiver is fabricated on a polyimide flexible substrate. The AM input signal is obtained from a signal generator (2.45GHz carrier signal) and transmitted by a horn antenna. The signal is received by the graphite antenna and demodulated using the GFET demodulator based on the ambipolar graphene characteristics at Dirac point. The output of the demodulator is connected to the speaker.

The schematic of the AM radio receiver is shown in Fig. 2.9. The input match network is used for impedance matching between the antenna (L_a,R_a) and GFET input impedance. The output matching network has two functions: i. impedance match between output of GFET and graphene speaker load (R_o) and ii. low pass filtering of the demodulated signal. Fig. 2.10 shows the fabricated receiver. The passive components – inductors, capacitors and resistors are currently realized using SMD components. The receiver measurements were carried out in a custom built anechoic chamber. Bending tests (30mm radius) were successfully carried out. The performance changes are small due to the flexibility of substrate, antenna, graphene FET and transmission lines.

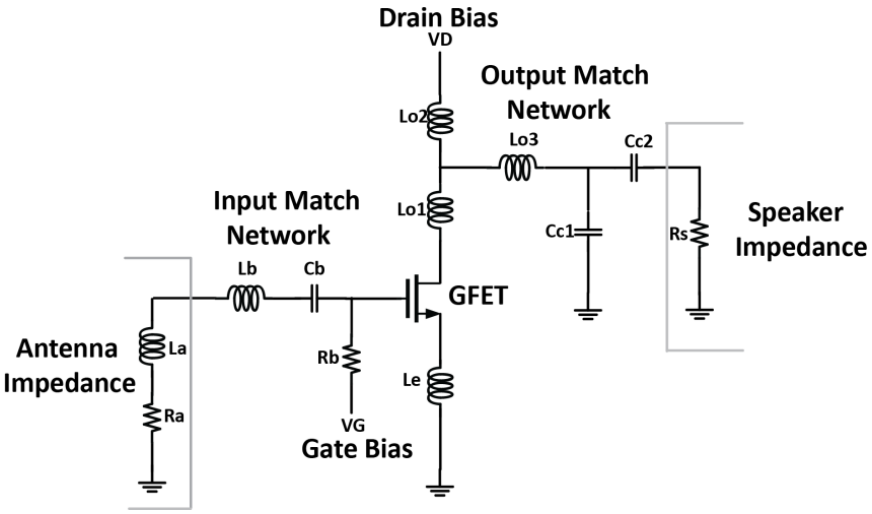

Figure 2.9. Schematic of graphene based AM radio receiver

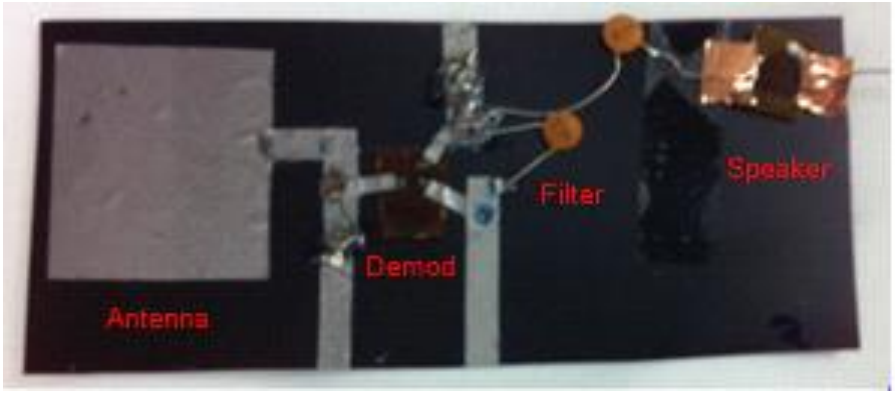

Figure 2.10. Fabricated AM radio receiver on flexible PI substrate. Reproduced from [14-15]

Table.1 gives the link budget of the flexible graphene receiver [8, 14]. The current AM receiver suffers from very high noise output due to lossy demodulator. To obtain larger signal to noise ratio and amplitude, a GFET low noise amplifier could be incorporated at the input. The performance could be further improved with optimized design of the demodulator and interconnects.

Path loss	**Graphite Antenna**	**GFET Demodulator Circuit**	**Total**
-1 dB/cm @ 6cm	**-5 dB**	**-35 dB**	**-46 dB**

Table 1: AM Radio link budget [14-15]

CONCLUSION

In this work we demonstrated state of the art flexible graphene transistor with f_T ~ 95GHz. We also demonstrated different RF building blocks (microstrip antenna, demodulator and speaker) for future graphene based RF receiver. Our results for graphene demodulator and speaker are promising for designing new flexible graphene nanosystems.

Chapter 3: MoS2 based Flexible Electronics

INTRODUCTION

Future flexible IoT based RF electronics requires transistors which operate at GHz frequency range and consume low power [1, 4]. Different materials (thin film amorphous silicon, organic semiconductors, graphene, IGZO) have be investigated for this application. Thin film amorphous silicon and organic semiconductors are ruled out due to their low mobility which limits their RF performance to MHz range [1, 3, 18]. Graphene has high mobility but lacks bandgap which prevents it from using for design of digital and RF circuits, which requires transistors to show good on/off ratio and current saturation. All these issues have been overcome by new 2D nanomaterial called Molybdenum Disulphide (MoS_2). This material belongs to a group of transition metal dichalcogens (TMDs). Monolayer MoS_2 has bandgap ~ 1.8eV, good mobility > 50cm^2/V.s, high current saturation, good on/off ratio ~ 10^6 and mechanical strength [1, 7]. In this work, we demonstrate large area monolayer flexible MoS_2 transistors operating at GHz frequency range and also show basic RF building blocks using those transistors.

GROWTH OF LARGE AREA MONOLAYER MoS_2

We grow large area monolayer MoS_2 using chemical vapor deposition (CVD) process (Fig 3.1a) [4]. The quality of the CVD MoS_2 is shown by the TEM image (Fig 3.1b) which clearly shows the lattice spacing of 2.7Å. Raman and photoluminescence (PL) measurements are done to determine the thickness of the as grown film (Fig 3.1c). PL peak at 1.8eV proves that the film is monolayer.

Note-This chapter results are published in the journals – 1. Sanne, A.; et.al; Radio Frequency Transistors and Circuits Based on CVD MoS2. *Nano letters* **2015,** *15* (8), 5039-45; 2. Chang, H. Y.; Large-Area Monolayer MoS2 for Flexible Low-Power RF Nanoelectronics in the GHz Regime. *Advanced materials* **2016,** *28* (9), 1818-23; 3. Sanne, Atresh, et al. "Embedded gate CVD MoS 2 microwave FETs." *npj 2D Materials and Applications* 1.1 (2017): 26; 4. Zhu et.al; Advancements in 2d Flexible Nanoelectronics: from material perspectives to RF applications. f*lexible and Printed Electronics*, IOP science, Aug 2017. I am coauthor on all these journals and contributed for many experimental results presented (Device fabrication, measurements, simulations).

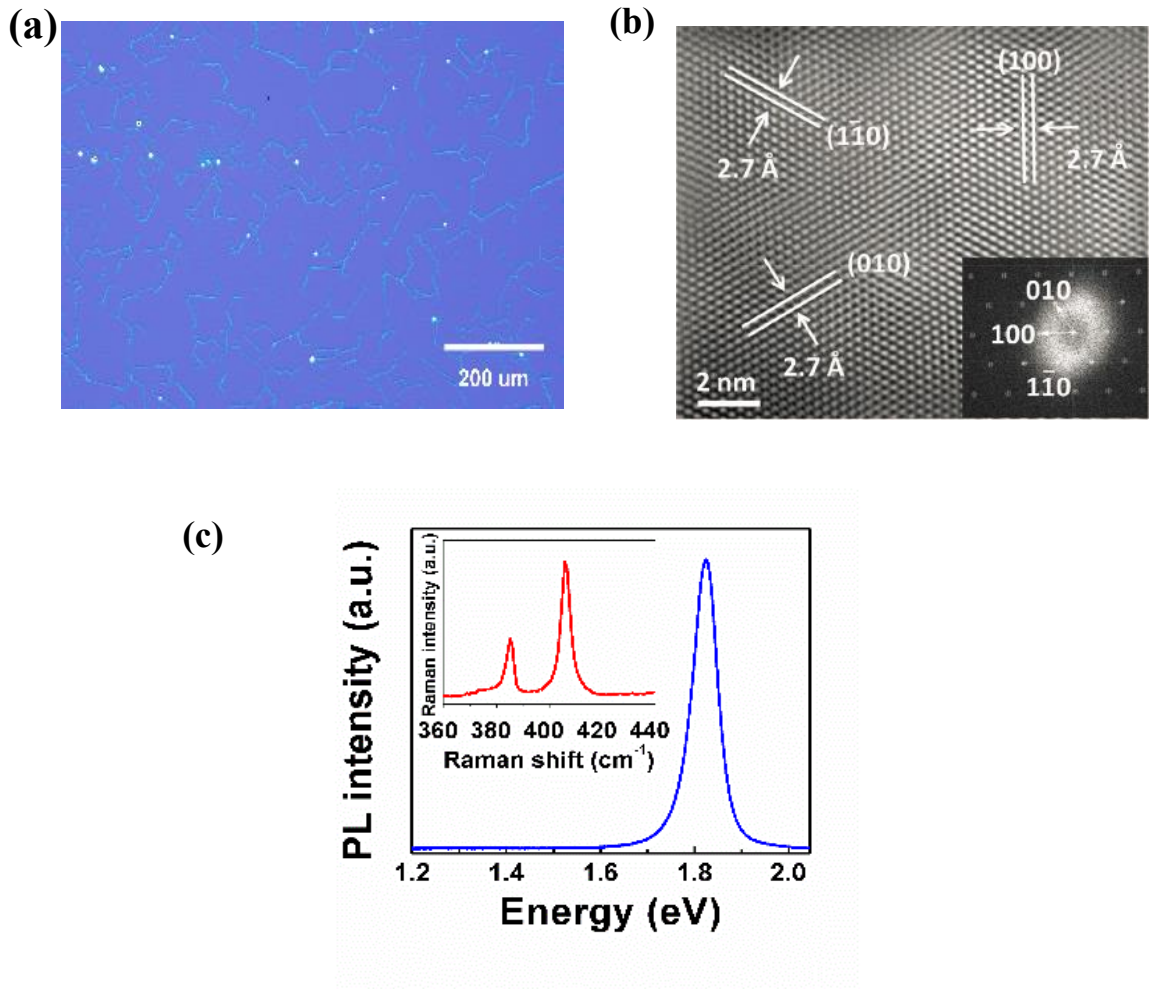

Fig. 3.1 (a) Optical microscope image of large area monolayer MoS_2. (b) TEM image of CVD MoS_2 with lattice spacing ~ 2.7Å. (c) Photoluminescence of monolayer MoS_2 (Inset shows Raman spectrum). Reproduced from [4]

FLEXIBLE MoS_2 TRANSISTOR FABRICATION AND CHARACTERIZATION

MoS_2 flexible transistor fabrication process involves transfer of CVD MoS_2 from SiO_2/Si substrate to flexible polyimide substrate using wet transfer process (see Fig 3.2a) [4]. We define source and drain contacts (Ag/Au – 20nm/20nm) using ebeam lithography (EBL) with channel length L ~ 500nm and width W ~ 10um. Top gate dielectric (ALD HfO_2 ~ 30nm thick) is used [19]. Pd (40nm) is used for top gate contact. Fig 3.2a inset shows the 3D illustration of our transistor. Fig.3.2b shows the transfer characteristics (I_D - V_G). Inset shows the output characteristics (I_D -V_D).

(a)

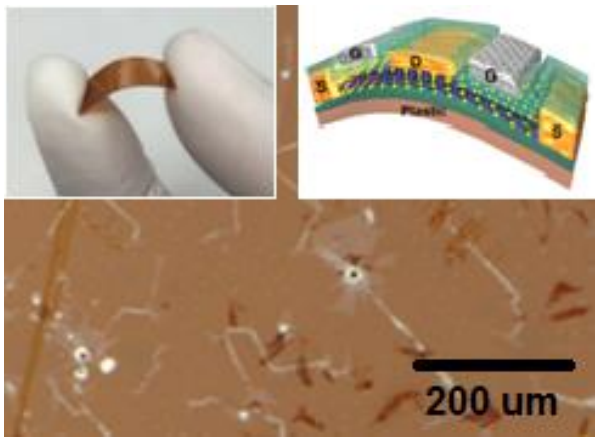

(b)

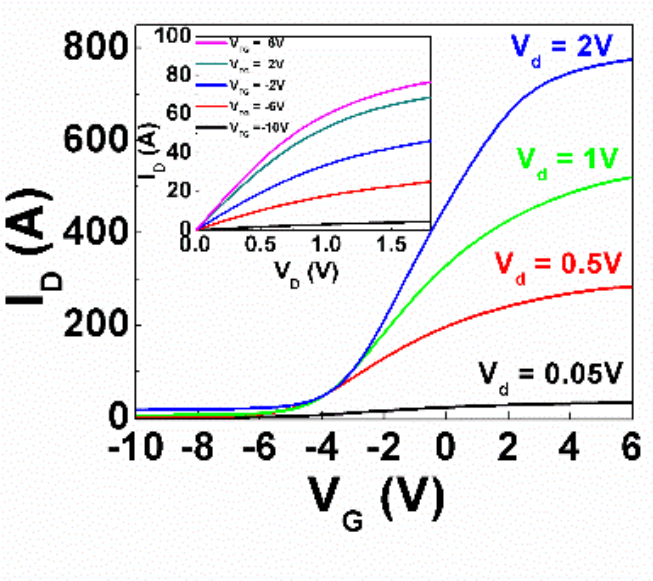

Figure. 3.2 (a) Optical image of MoS_2 transferred to polyimide (PI) substrate. Inset shows the schematic of flexible transistor. (b) Transfer characteristics of flexible MoS_2 transistor (L =500nm, W=10um). Inset shows the I_D-V_D characteristics with good current saturation.

We designed and fabricated top gate and embedded gate CVD MoS_2 transistors on Si/SiO2 substrate. Fig 3.3 (a,b) shows the optical image and cross section image of top gate MoS_2 transistor (Lg ~ 250nm) and Fig 3.3c shows the fabrication flow. Fig 3.4(a,b) shows the transfer and output characteristics of top gate MoS_2 transistor. These devices shows mobility ~ 55cm2/V.s, peak trans-conductance gm ~ 38uS/um, Ion/Ioff ratio ~ 10^6, maximum current density Id ~ 200uA/um and contact resistance Rc ~ 2.5kOhms.um [7, 20,40].

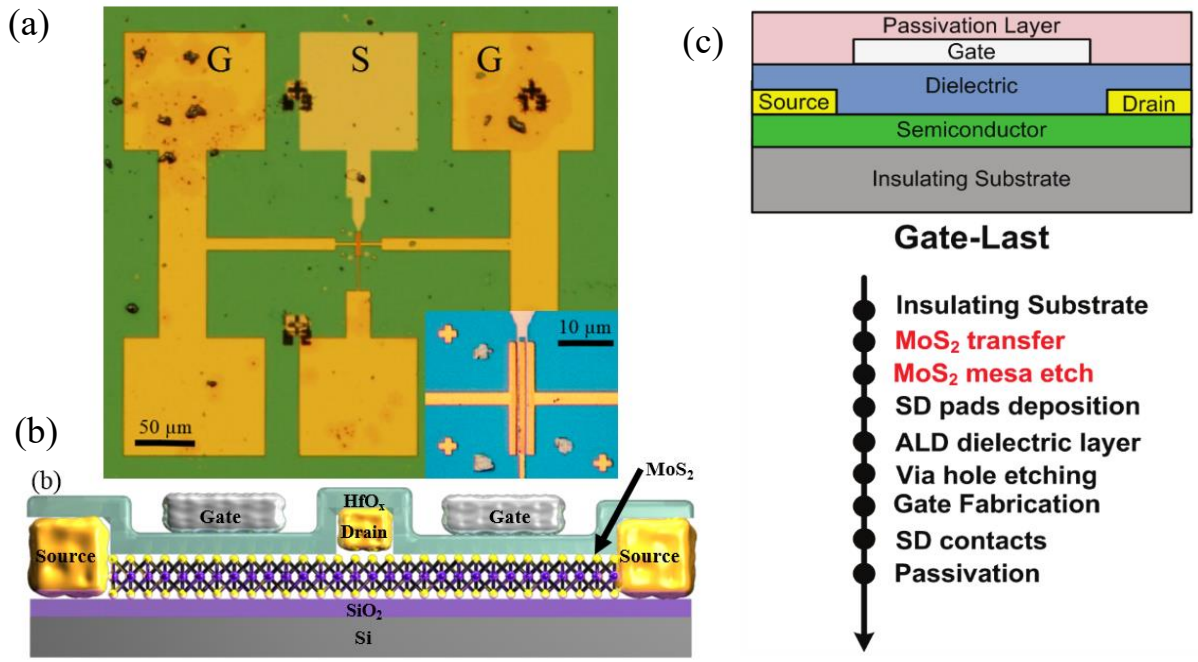

Figure 3.3: (a) optical image of MoS_2 transistor. (b) cross sectional image of dual fingered MoS_2 transistor. (c) Fabrication flow of top gate MoS_2 transistor. Reproduced from [7, 20]

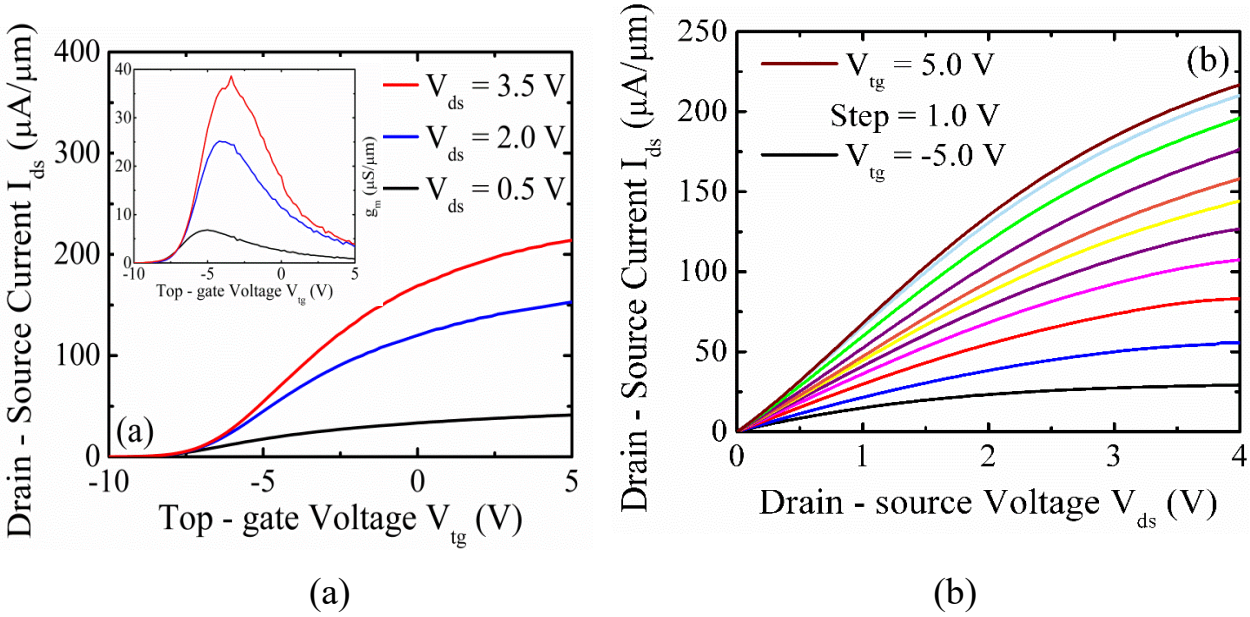

(a) (b)

Figure 3.4: (a) Transfer characteristics of flexible MoS_2 transistor (L =250nm, W=20um). (b) I_D-V_D characteristics with good current saturation. Reproduced from [7, 20].

We later tried fabrication of embedded gate MoS_2 transistor (Lg ~ 150nm) to obtain better device performance (DC and RF) compared to top gate transistors. This enhancement in device performance comes due to good electrostatic gating and also due to MoS_2 thin film not subjected to many fabrication steps. Fig 3.5 (a,b) shows the optical image and cross section image of top gate MoS_2 transistor (Lg ~ 150nm) and Fig 3.5c shows the fabrication flow. Fig 3.6 (a,b) shows the transfer and output characteristics of top gate MoS_2 transistor. These devices shows mobility ~ 82cm2/V.s, peak trans-

conductance gm ~ 70uS/um, Ion/Ioff ratio ~ 10^8, threshold voltage Vth ~ 0.5V and reasonable good contact resistance Rc ~ 3.5kOhms.um [21]

(a)

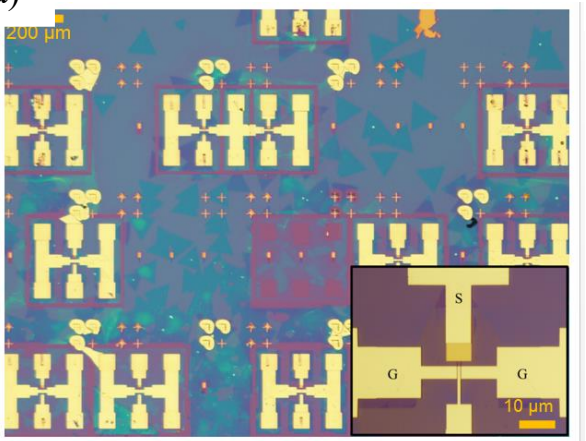

(b)

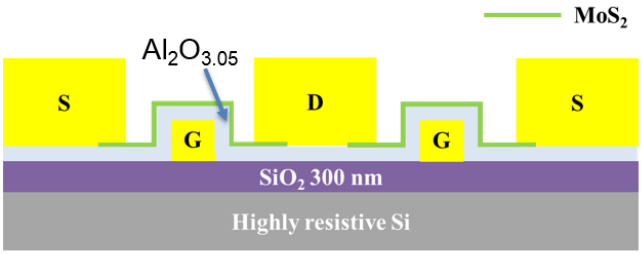

(c)

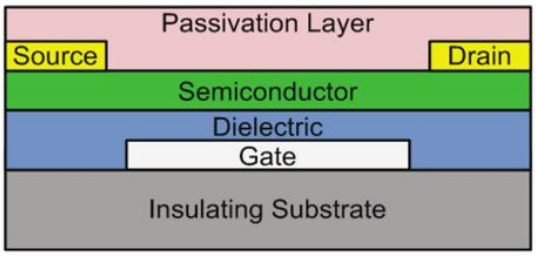

Gate-First

- Insulating Substrate
- Gate Fabrication
- ALD dielectric layer
- FG annealing
- Via hole etching
- SD pads deposition
- MoS_2 transfer
- MoS_2 mesa etch
- SD contacts
- Passivation

Figure 3.5: (a) Optical image of MoS_2 transistor. (b) Cross-sectional image of dual fingered MoS_2 transistor. (c) Fabrication flow of top gate MoS_2 transistor. Reproduced from [21]

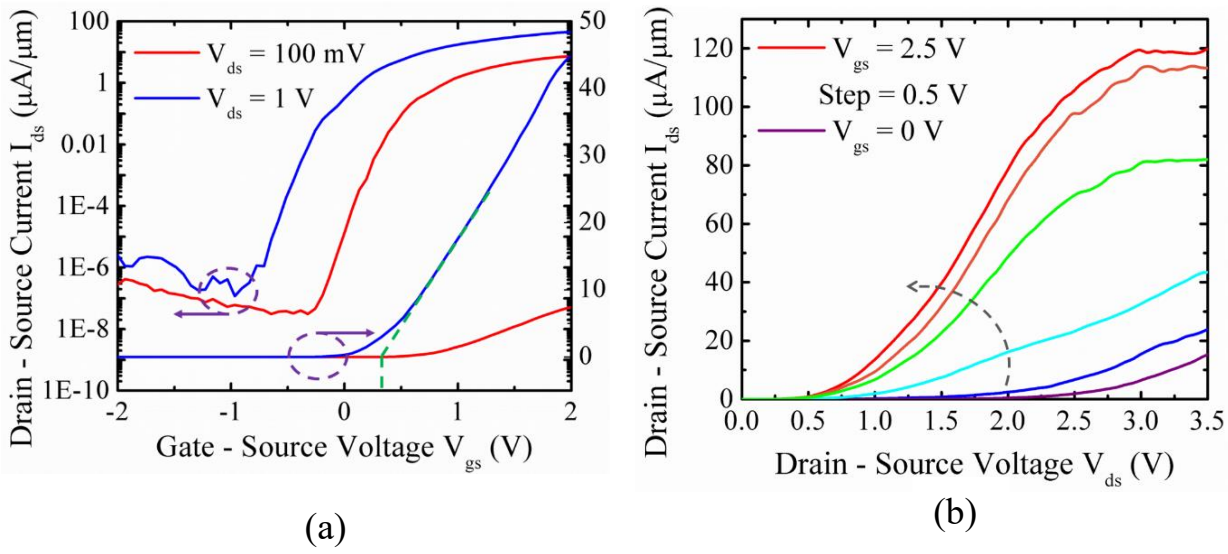

Figure 3.6: (a) Transfer characteristics of flexible MoS_2 transistor (L =250nm, W=20um). (b) I_D-V_D characteristics with good current saturation. Reproduced from [21]

FLEXIBLE MoS_2 TRANSISTOR RF PERFORMANCE

RF measurements of flexible MoS_2 transistors were carried out using Agilent vector network analyzer (VNA) and cascade probe station. RF performance is determined by frequency (f_T) at which current gain (h_{21}) becomes unity and also frequency (f_{MAX}) at which power gain becomes unity. After de-embedding (see Appendix A.1) we achieved a record f_T ~ 5.9GHz and f_{MAX} ~ 3.3GHz (See Fig 3.7a,b). These values are comparable to our earlier results on transistors fabricated on as grown monolayer MoS_2 on SiO_2/Si substrate [7]. This shows that the transfer process has not degraded the quality of MoS_2.

We also performed RF measurements of our transistors under compressive and tensile strain. The device were operational for compressive strain of 3% with slight degradation of f_T (Fig 3.7c).

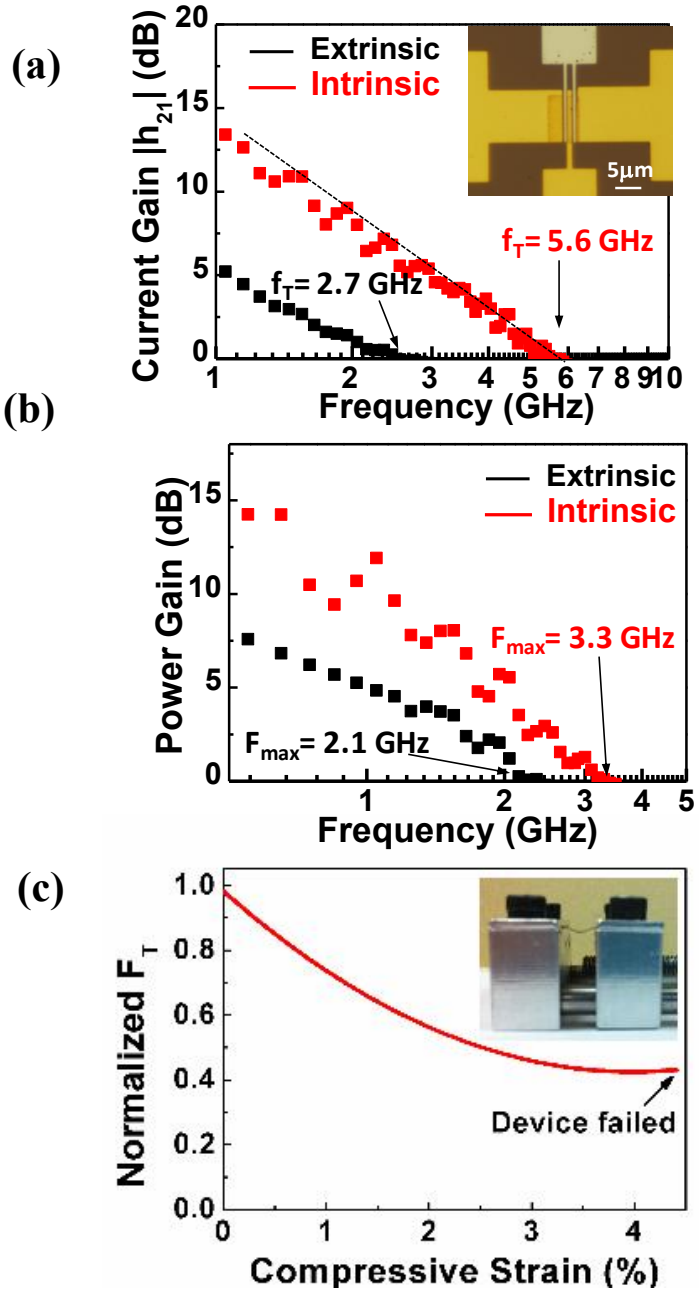

Figure 3.7: Flexible MoS_2 transistor RF performance. .(a) f_T ~ 5.9 GHz for transistor (L = 500nm, W = 10um). (b) f_{MAX} ~ 3.3GHz (c) RF performance under strain. Inset shows the tool used for strain measurement. Reproduced from [4, 12, 40]

As discussed in section 3.4, we did RF characterization of both top gate and embedded gate MoS_2 transistors. Top gate dual fingered MoS_2 transistors demonstrate intrinsic f_T ~ 6.7GHz and f_{MAX} ~ 5.3GHz (see Fig 3.8 (a,b)). Embedded gate MoS_2 transistor demonstrate record intrinsic f_T ~ 20GHz and f_{MAX} ~ 11.4GHz (see Fig 3.9 (a,b)). This enhanced RF performance of embedded gate MoS_2 transistor is attributed to good quality of CVD MoS_2 film, good electrostatic gate control and minimum degradation of MoS_2 film during device fabrication. Table 1 shows a comparison of RF performance of published MoS_2 transistors works.

I acknowledge Sherry Chang, Atresh Sanne and Saungeun Park's contribution to top gate and embedded gate device fabrication and characterization. Interested reader can refer to journals published on this works [7, 12, 40].

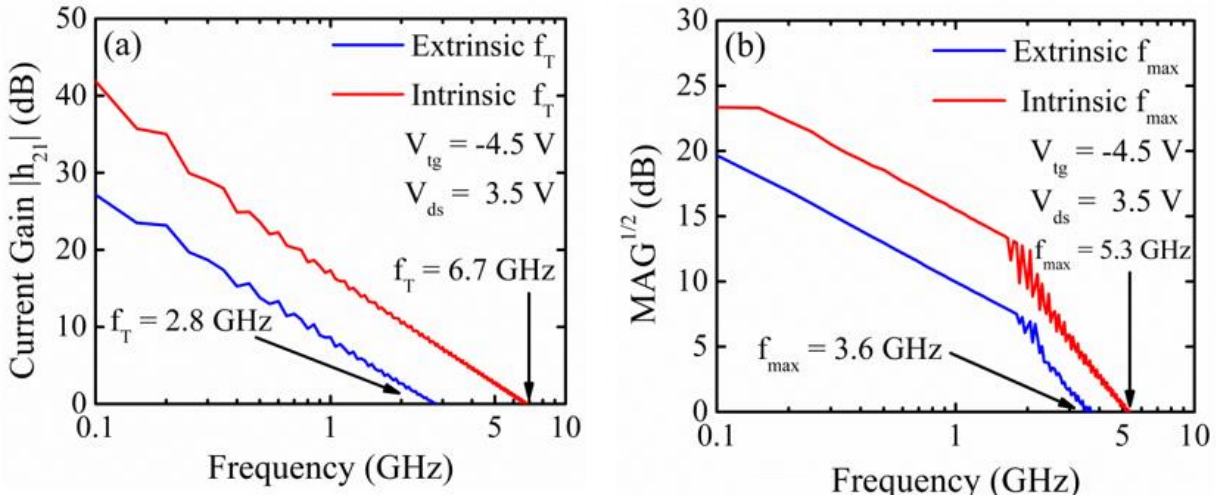

Figure 3.8: Top gate MoS_2 transistor RF performance. .(a) f_T ~ 6.7 GHz for transistor (L = 250nm, W = 20um). (b) f_{MAX} ~ 5.3GHz. Reproduced from [7, 20]

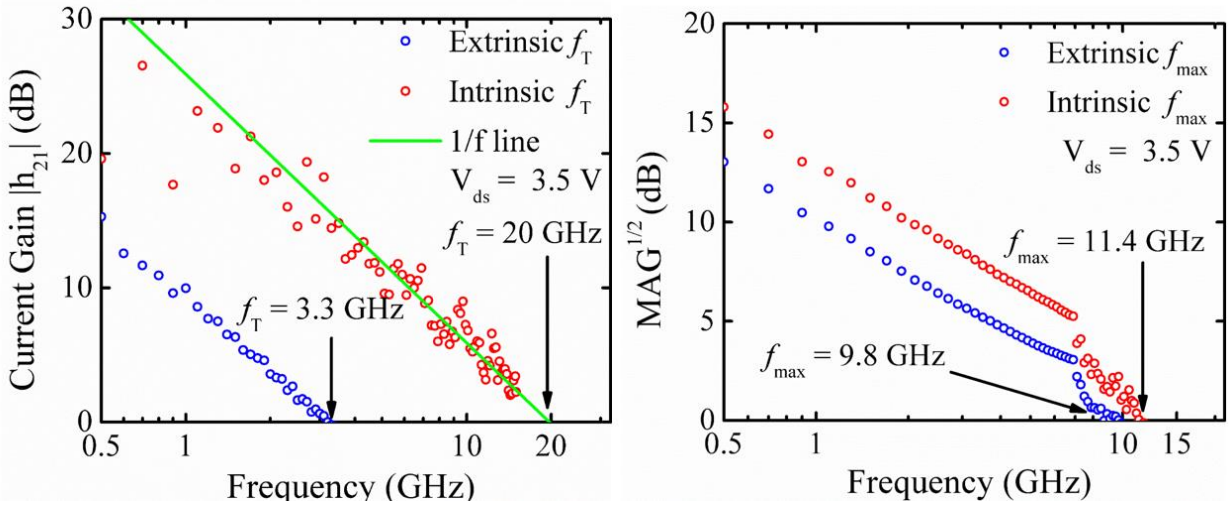

Figure 3.9: Embedded gate MoS_2 transistor RF performance. .(a) f_T ~ 20 GHz for transistor (L = 140nm, W = 10um). (b) f_{MAX} ~ 11.4GHz. Reproduced from [21, 41]

Device Configuration (active/substrate/structure)	**f_T ext/int (GHz)**	**f_{max} ext/ int (GHz)**	**A_v ext/ Int (GHz)**	**L_g (nm)**	**V_d (V)**	**v_{sat} ($\times 10^6$ cm/s)**
CVD 1L/Si/ embedded gate	3.3/20	9.8/11.4	4.6/19.5	150	3.5	1.88*
Exf 3L/Si/ top gate	6/25	-/16	-/45	70	2.5	1.1
Exf 2-7nm/Si/ transferred gate	-/42	-/50	-/-	68	5	1.79
CVD 1L/Flex/ top gate	2.7/5.6	2.1/3.3	-/-	500	2	1.76
CVD 1L/Si/ top gate	2.8/6.7	3.6/5.3	3/11	300	3.5	1.26

Table 2: Comparison of RF performance of both CVD and exfoliated MoS_2 transistors.

FLEXIBLE MoS_2 TRANSISTOR BASED RF CIRCUITS

Having obtained good DC and RF performance from flexible MoS_2 transistors, motivated us to design basic RF circuits to be used within an IoT system. We designed common source (CS) RF amplifier as shown in Fig 3.10a. This amplifier is biased at peak transconductance point. We obtained a gain of 15dB. This amplifier can be modified to be used as low noise amplifier in RF receiver with proper sizing of transistors. With proper measurement setup and impedance matching network, we can demonstrate RF amplifier at GHz range.

Fig 3.10b shows the single FET active RF mixer with conversion gain of -17dB. We feed RF and LO signal to the gate input of our transistor using power combiner. The transistor is biased in nonlinear regain. The up-converted or down-converted signal is tapped at the drain output. Additional filters can be used at the input and output to improve signal isolation (RF-LO, LO-IF isolation).

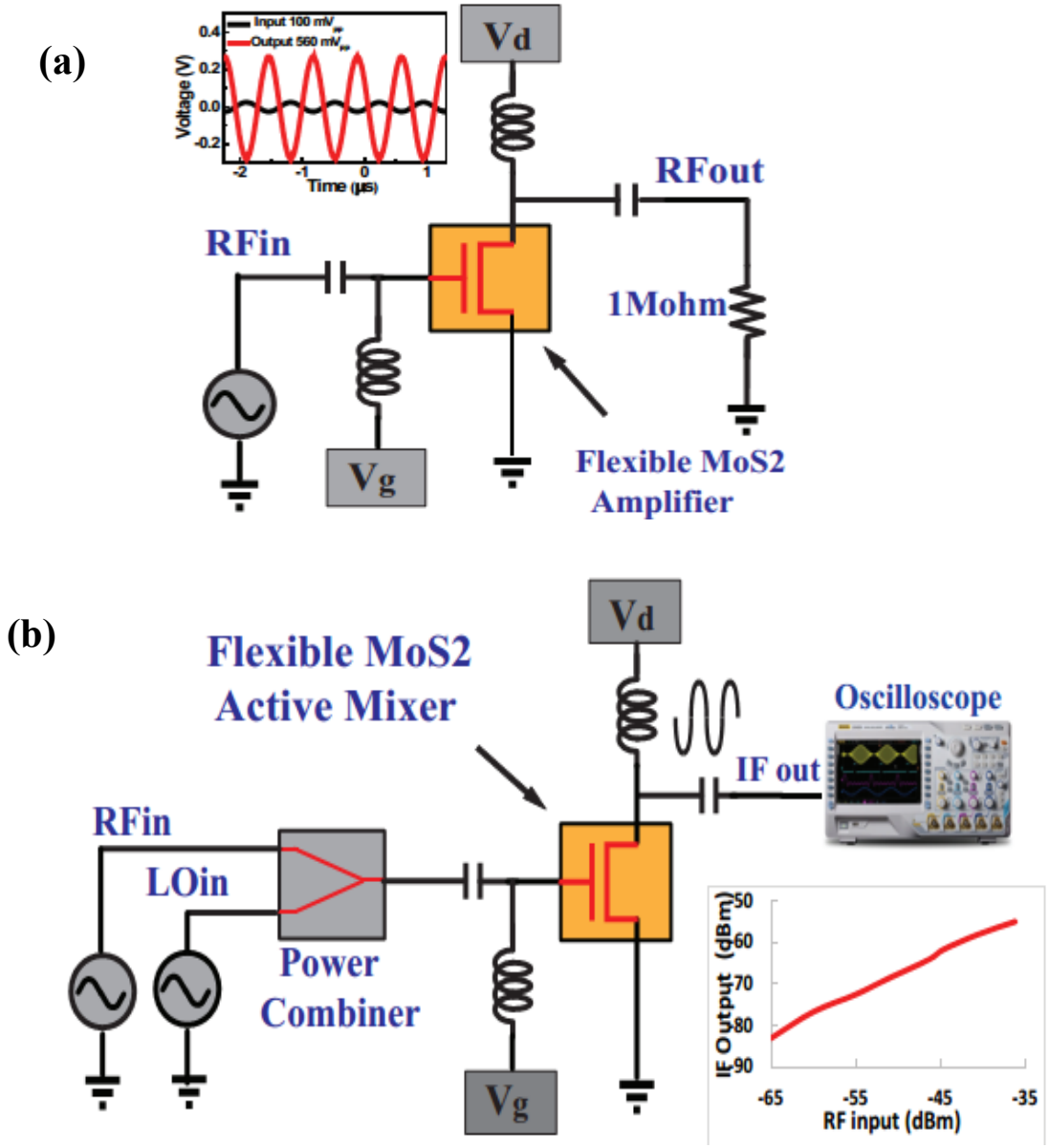

Figure 3.10 (a) Schematic of common source amplifier. Inset shows waveforms (input – black, output – red). (b) Schematic of single FET active mixer. Inset shows conversion gain plot (RF –IF).

We also demonstrate wireless AM demodulator using flexible MoS_2 transistor as shown in Fig 3.11. The working principle is similar to RF mixer. The transmitted AM signal (carrier @ 1.5MHz, modulating signal @ 1MHz, modulation depth – 50%) is received by dipole antenna and is power combined with local carrier @ 1.5MHz and fed to gate input of demodulator. The demodulated output is obtained by low pass filtering the drain output. Fig 3.11 inset shows the FFT of demodulator output. This result is very promising for design of future flexible cell phones.

Interested readers are recommended our recently published papers [4, 7] on this work for more details on design, fabrication, measurements and analysis.

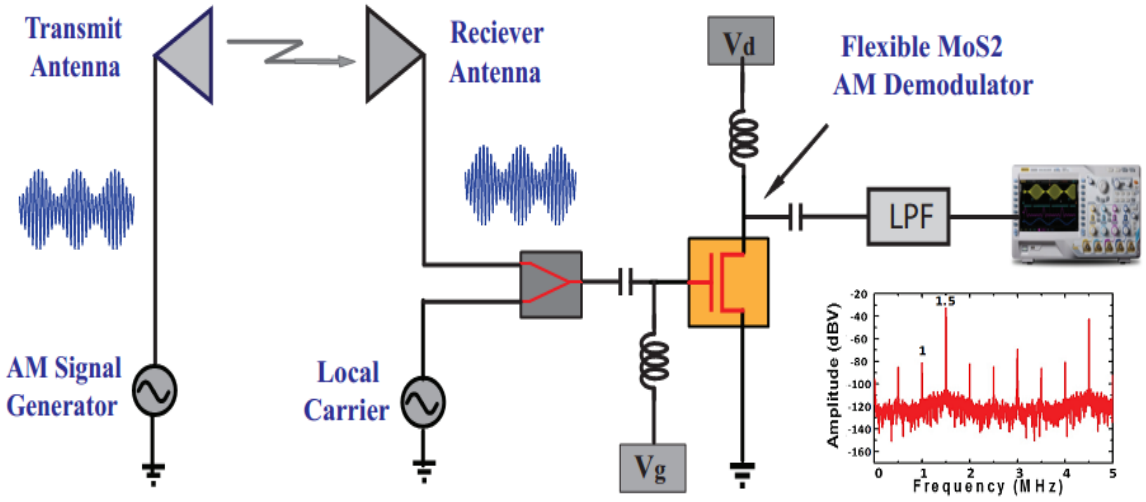

Figure 3.11 Schematic of AM demodulator using flexible MoS_2 transistor. Inset shows the FFT of AM receiver output.

As discussed in section 3.3 and 3.4, top gate devices show high mobility, current saturation, GHz frequency performance (f_T and f_{MAX}), and high voltage gain. This motivated us to design analog circuits – amplifier and mixers. We designed common source (CS) amplifier and an active mixer using top gate MoS_2 transistors. Fig 3.12a shows the schematic of CS amplifier and Fig 3.12b shows the input and output waveforms. RF input was applied to gate input and amplified output was tapped at drain output. MoS_2 transistor was biased at peak transconductance point to get maximum gain ~ 14dB. We have shown in section 3.6.2 potential of MoS_2 transistor by design of cascode amplifier which shows gain of ~ 15dB @ 1.2GHz. This is very promising for IOT and low power sensor applications.

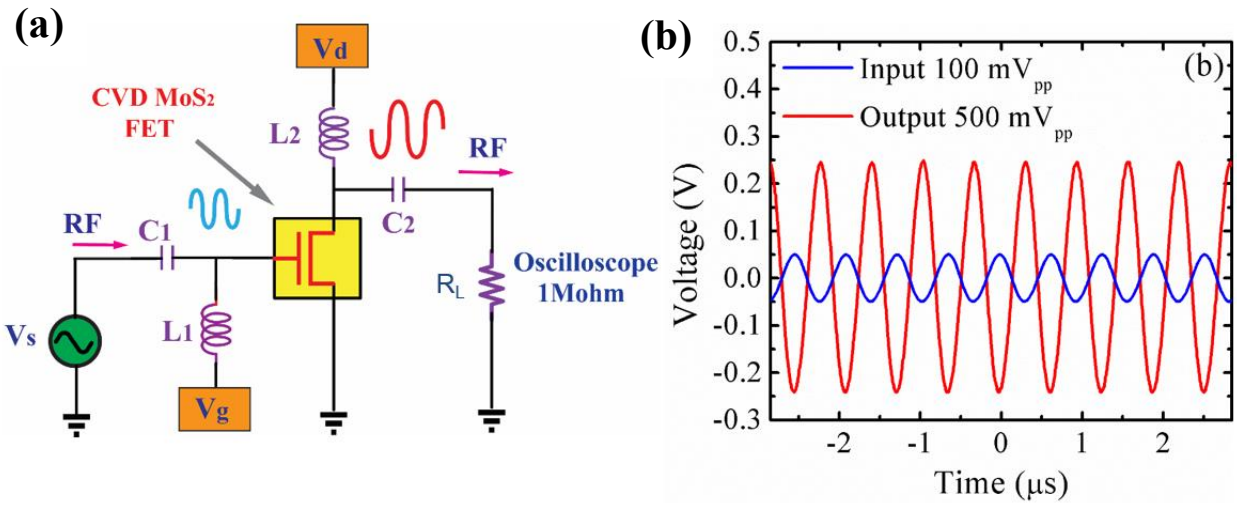

Figure 3.12: (a) Schematic of common source amplifier. (b) Shows input (blue) and output waveforms.

We designed and measured for the first time MoS_2 transistor based single FET active mixer. Fig 2.13a shows the schematic of this mixer. We have biased MoS_2 transistor in deep saturation where drain current has nonlinear relationship with input gate voltage. RF and LO signals are power combined and applied to gate input. Output (down-converted IF signal at RF-LO) is tapped at drain output. A low pass filters can be used to attenuate high frequency components from IF signal. This mixer shows a conversion gain of ~ -15dB. Fig 2.13b,c shows mixer output FFT spectrum and conversion gain plot (refer to appendix A.2 for theoretical analysis of mixer operation). Fig 2.13d shows RF mixer measurement setup. These results are very promising for design of wireless receivers.

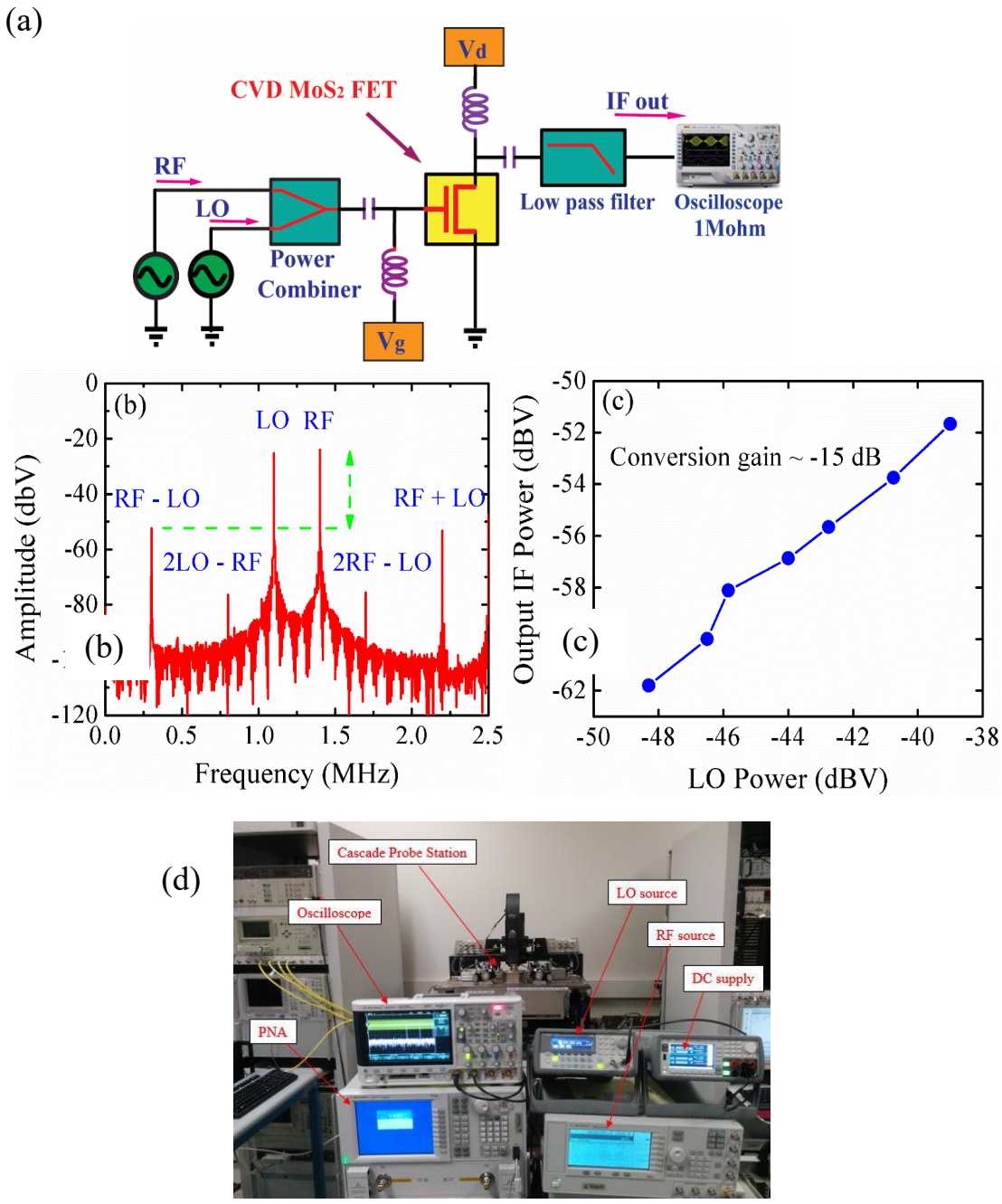

Figure 3.13: (a) Schematic of single FET active mixer. (b) FFT spectrum of mixer output. (c) Shows conversion gain plot (RF –IF). (d) Mixer measurement setup. Reproduced from [4, 12]

MODELING OF MoS_2 TRANSISTORS

We show here MoS_2 transistor models which can be used for design of integrated circuits. Having obtained good DC and RF performance from MoS_2 transistors, motivated us to design small signal RF model for MoS_2 transistor, MoS_2 S-parameter model based RF amplifier at 1.2GHz, and MoS_2 MVS model based mixed signal circuits. These models can be used in circuit simulation tool like Cadence and ADS for design of integrated circuits. Fig 3.14 shows the flow associated with design and validation of MoS_2 based chip. It starts with synthesis of large area CVD monolayer MoS_2, followed by design and fabrication of MoS_2 transistors, design of Mos2 transistor model using transistor characterization results (DC and RF), design of integrated circuits using those models in circuit simulation tool, optimize those circuit results, design layout, and finally fabricate MoS_2 chip and perform validation.

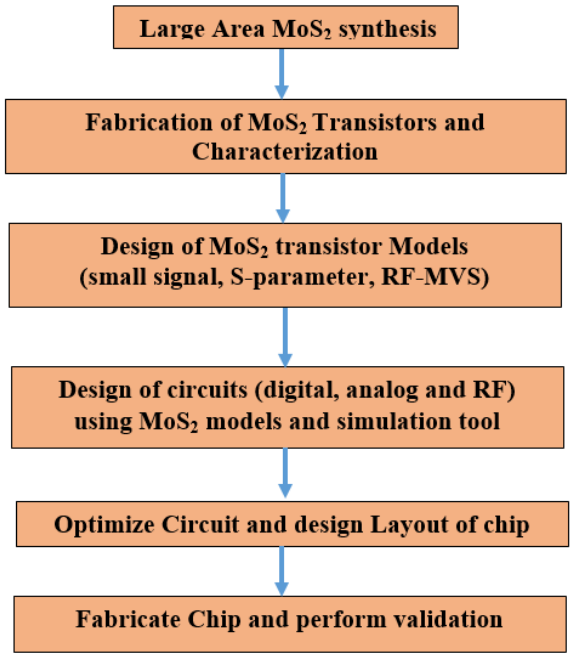

Figure 3.14: Flow chart for design of MoS_2 chip and validation

Design of Small Signal RF Model

We designed a simple small signal RF Model for top gate MoS_2 transistor. This model parameters are obtained from measured S parameters (device under test-DUT, open and short structures). The equations mentioned in [22] can be used to obtain intrinsic model parameters. RF passives component (L_g, R_g, L_s, R_s, L_d, R_d) values can be obtained by numerical analysis based upon S-parameter results of open and short structures. Having obtained both intrinsic and extrinsic model parameters, we can now use small signal model (see Fig 3.15) in commercial RF simulation software (Agilent ADS) to design RF circuits. This model gives us information about how device parameters affect overall circuit performance. Fig 3.16 shows the f_T and f_{max} obtained from this small signal RF model of MoS2. These plots approximately matches with experimental results. The results are promising for low frequency receiver application. This model results can be further optimized by adding additional parasitics and also running optimization algorithms.

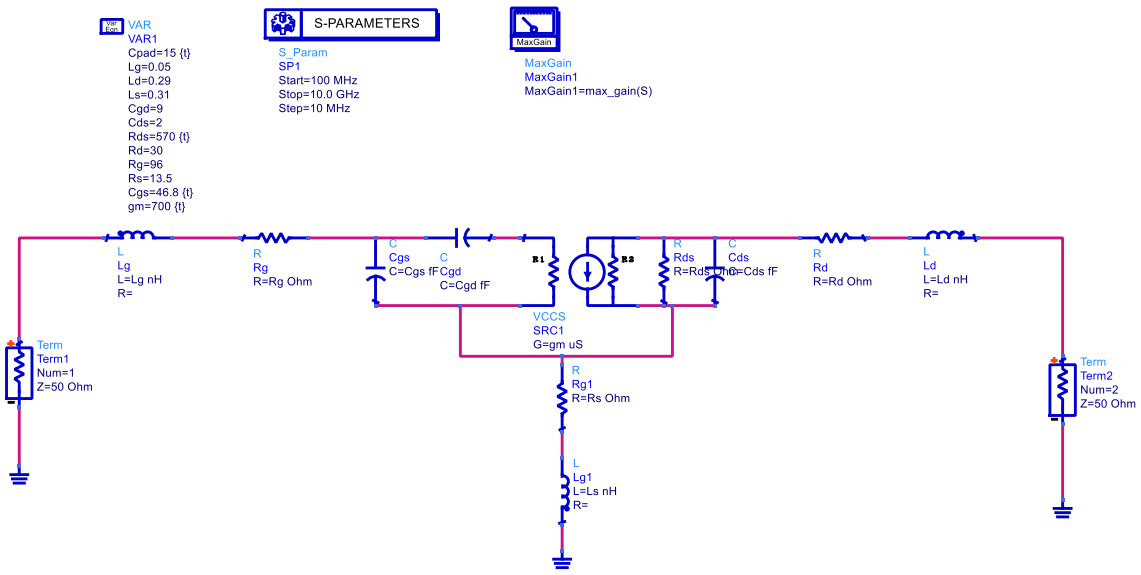

Figure 3.15: Small signal model of MoS2 transistor

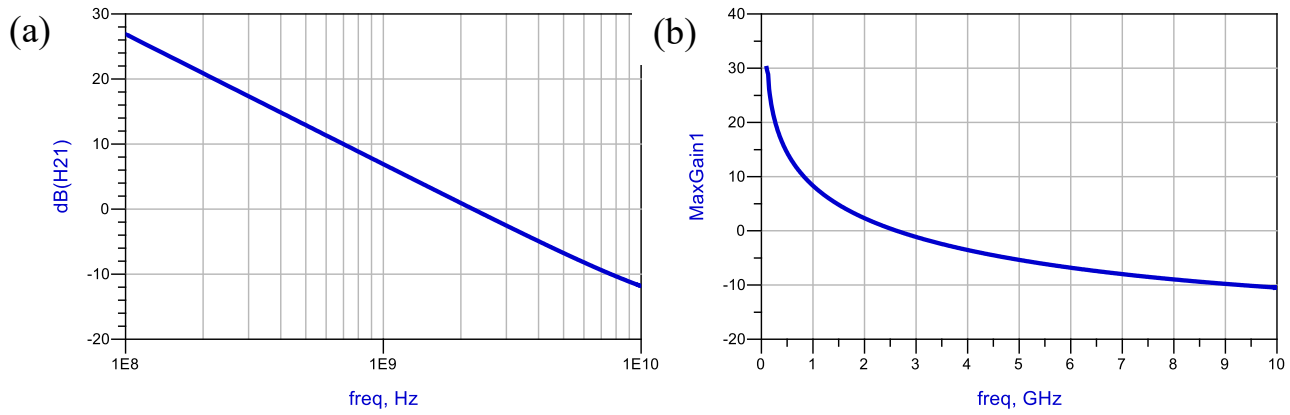

Figure 3.16: f_T and f_{MAX} results of MoS2 RF small signal model

Design of Cascode Amplifier using S-parameter Model

Using the as-measured S-parameters, we designed a RF amplifier to demonstrate CVD MoS_2 as a viable material for a front-end low noise amplifier (LNA). We chose a cascode topology to minimize the Miller effect, provide input-output isolation, and improve the overall gain-bandwidth product. The amplifier schematic is shown in Fig 3.17(a). Fig 3.17(b) shows the amplifier gain (S_{21} in dB) and the input match (S_{11} in dB). We see a gain greater than 15 dB operating at 1.2 GHz, attributed to good current saturation. Fig 3.18(c) shows the input-output isolation greater than 20 dB at 1.2 GHz as afforded by the cascode topology. The high gain of our front-end amplifier helps with setting the noise floor of the RF receiver. An input match network (IMN) is designed for matching the input impedance (Z_{in}) to the source impedance, R_s = 50 Ω. With the IMN we see input return loss greater than 10 dB. An output match network (OMN) is employed to improve the gain over the frequency bandwidth of 1.1-1.3 GHz. A standard Chebyshev N-order band pass filter topology can be modified for the design of the match networks[23]. We plan to further improve this design to take into account noise parameters for the practical design of MoS_2-based GHz LNAs.

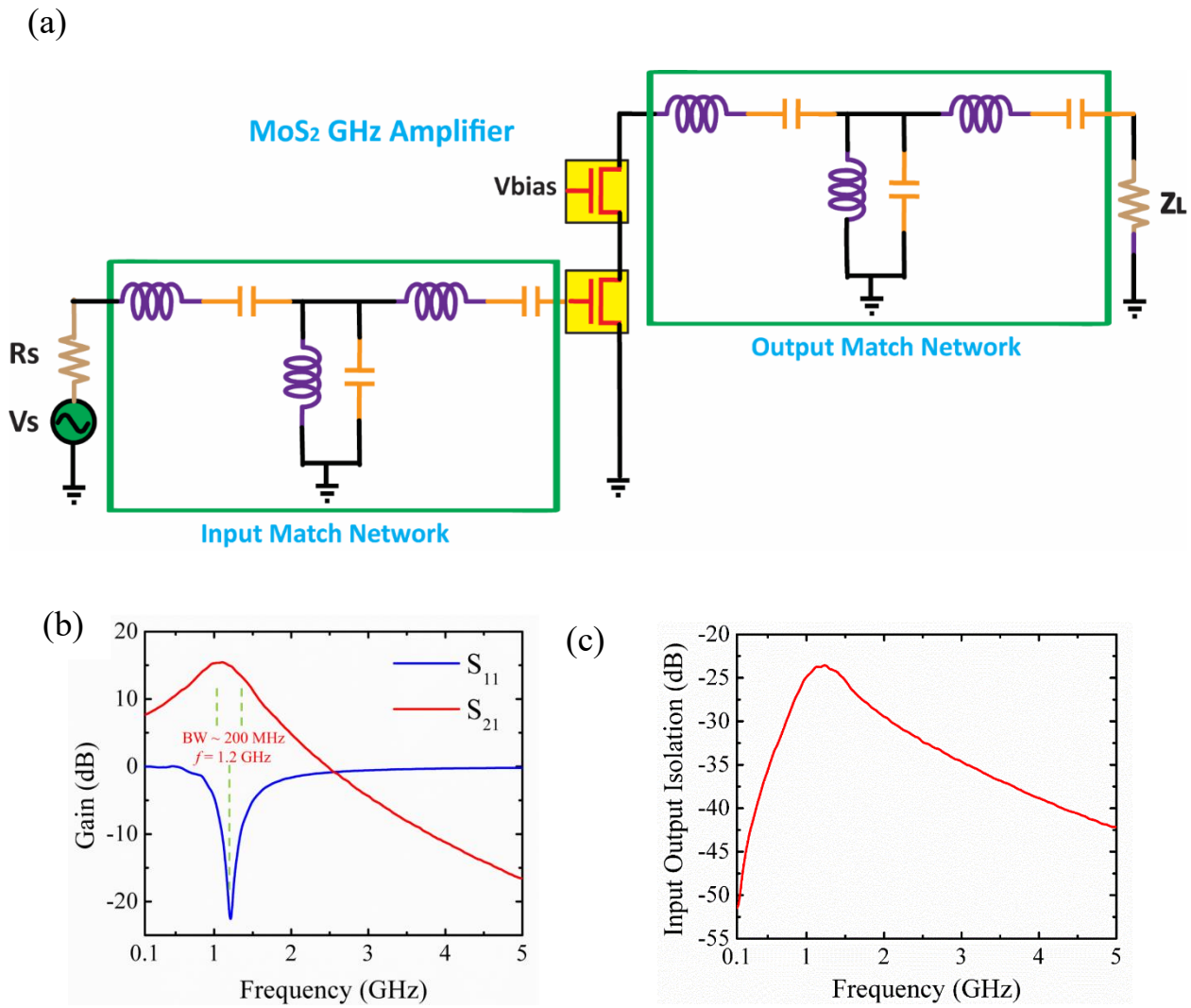

Figure 3.17: (a) Schematic of cascode amplifier using S-parameter model of MoS2 transistor. (b) Amplifier gain (S21 in dB) and input match (S11 in dB). (c) Input-Output isolation (S12in dB) – Reproduced from Ref [41]

Design of Analog Circuits using MVS MoS2 model

Additionally, we have shown here the design of three commonly used mixed-signal circuits – track and hold circuit (Fig.3.18a), full wave rectifier (Fig. 3.18b), and an AM envelope detector (Fig. 3.18c) using our MVS model for MoS_2 transistor [24]. The track and hold circuit, used for analog to digital conversion, shows a thermal noise limited SNR of 90.85 dB. The full wave rectifier, used for AC to DC conversion, can be coupled with a reservoir capacitor for a smooth DC signal. The AM envelope detector is used for the demodulation of AM radio signal, and here shows a peak attenuation of 13.8 dB.

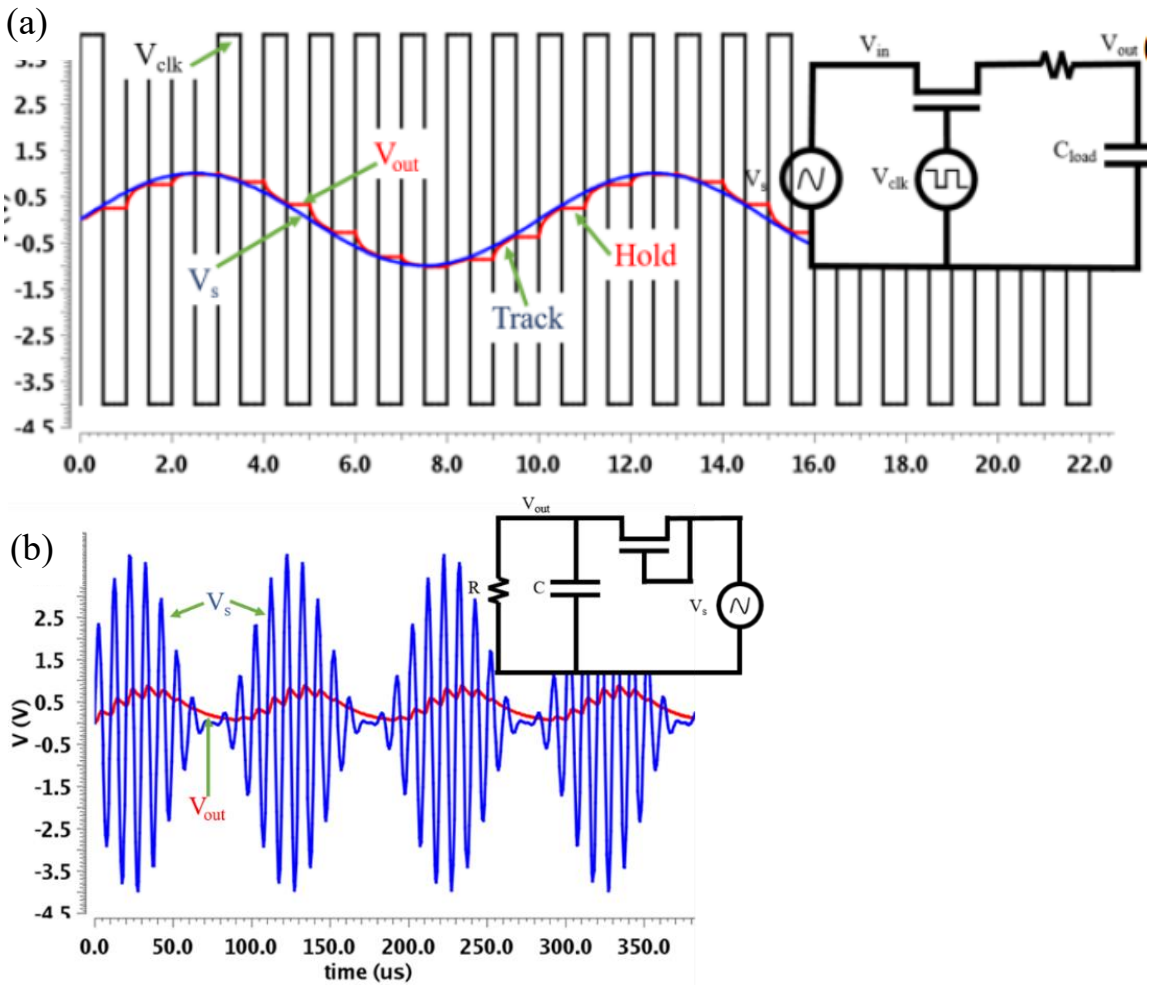

(c)

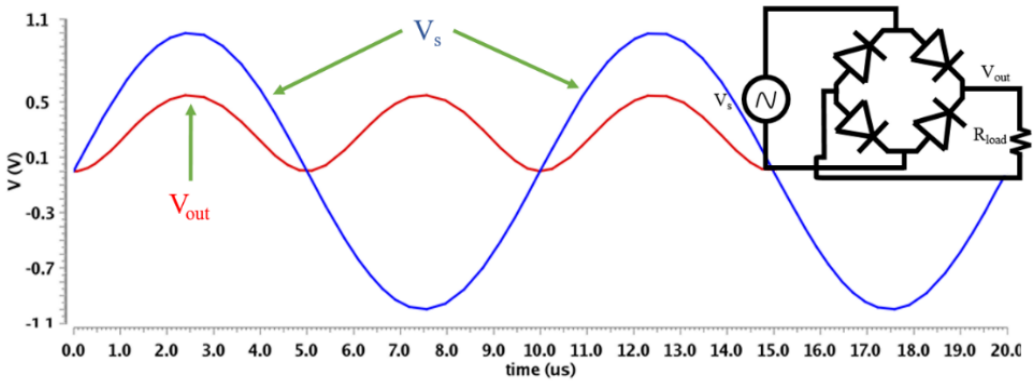

Figure 3.18: Schematics of mixed –signal circuits. (a) Track and hold circuit. (b) AM envelope detector. (c) Full wave rectifier.

CONCLUSION

In this work, we have shown for the first time GHz performance from monolayer CVD MoS2 transistors. We also demonstrated basic RF circuits (amplifiers, mixers and demodulators) which are going to be part of a flexible IoT receiver.

PART2: *PLASMONICS USING 2D NANOMATERIALS*

Chapter 4: Graphene Plasmonics

MULTIBAND GRAPHENE METASURFACES BY MOIRÉ NANOSPHERE LITHOGRAPHY

Graphene, one of the most exciting two-dimensional (2D) materials, has shown extraordinary optical properties due to the strong surface plasmon polaritons supported by graphene nanostructures [25-27]. Graphene metasurfaces show plasmonic resonance bands that can be tuned from mid-infrared (MIR) to terahertz (THz) regime [25]. [28-29] have shown patterned graphene based plasmonic devices for bio sensing, spectroscopy and light modulation applications.

The current graphene plasmonic metasurfaces are usually single-band. Plasmonic metasurfaces with multiband resonance peaks have proven to be extremely effective in molecular detection with ultrahigh sensitivity and accuracy. Multiband devices at variable electromagnetic spectra are also highly desired to meet the strong demand for the ever-increasing accuracy and high speed in surveillance and communication systems. Herein, we demonstrate an effective method to pattern graphene grown by chemical vapor deposition (CVD) into moiré metasurfaces with gradient nanostructures.

The graphene is patterned into moiré metasurfaces via combination of our previously developed moiré nanosphere lithography (MNSL [30-31] with O_2 reactive ion etching (RIE), as shown in Fig. 4.1(a)-(c). In brief, colloidal PS nanospheres are self-assemble into monolayer on substrates with graphene. A second monolayer of PS nanospheres is then deposited on top of the first PS monolayer via similar process. The relative rotation angle between the first and second PS monolayer can be controlled to obtain various moiré patterns. The following RIE with O_2 creates voids between closely packed nanospheres and etches away graphene that are exposed to O_2 plasma by voids.

Note-This chapter results are published in the following journals – 1. Wu, et.al; Tunable and Gradient Graphene Metasurfaces by Self-assembly-based Moiré Nanosphere Lithography. *Adv Opt Mat* **2016**; 2. Katsumata, et.al; Large area fabrication of graphene nanoribbons by wetting transparency-assisted block copolymer lithography. *Polymer* **2017,** *110*, 131-138. I am coauthor on both journal and contributed significantly for many experimental results presented (device fabrication and measurements).

After removal of the residue nanospheres, graphene sheets with moiré patterns are then left on substrates, as shown in the SEM images in Fig. 4.1d

By varying the relative rotational angle between top and bottom monolayers of PS nanosphere during MNSL, the resulting nanopatterns are considerably expanded in comparison to conventional nanosphere lithography applying only one monolayer of PS nanospheres as etching mask. Fig. 4.2(a) - (c) show the SEM images of the graphene sheets with moiré patterns fabricated with different relative rotation angles of 7.5°, 12°, and 19°, respectively. It can be observed that the size and shape of the graphene nanostructures in the metasurfaces change significantly with increasing relative rotation angle. Our results demonstrate that graphene moiré metasurfaces with gradient and complex moiré patterns can be controllably fabricated by our methods.

Graphene metasurfaces support surface plasmon with resonance wavelength that is highly dependent on the shape and size of the nanostructures. Under light illumination, the surface plasmon resonances can be excited, as shown in Fig. 4.2(d). Due to the large gradient and the high complexity of graphene moiré metasurfaces, they are promising candidates for tunable multiband plasmonic devices. We prove this by measuring the transmission extinction of graphene moiré metasurfaces with different patterns. As shown in Fig. 4.2(e), the number and the wavelength of resonance peaks of the graphene metasurfaces are highly dependent on the patterns. Interested readers are recommended to refer to our recently published paper [32] on this work for more details.

This work is done in collaboration with Prof. Yuebing Zheng's group (ME Dept, UT Austin). I acknowledge Zilong Wu and Wei Li's contribution to this work.

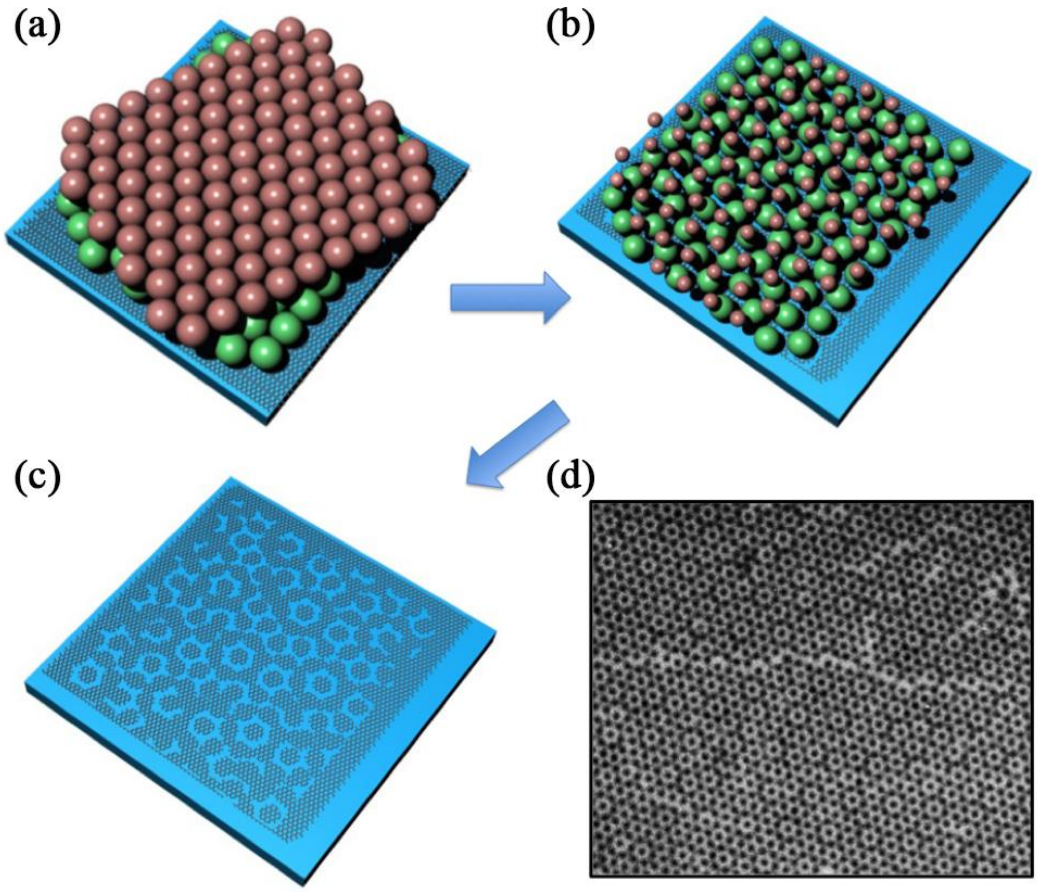

Figure 4.1 (a-c) Schematics of fabrication processes of graphene moiré metasurfaces on Si substrates (blue). θ demonstrates the relative rotation angle between the bottom (green) and top (red) monolayers of nanospheres. (d) SEM figures of a representative graphene moiré metasurface. Reproduced here from [32]

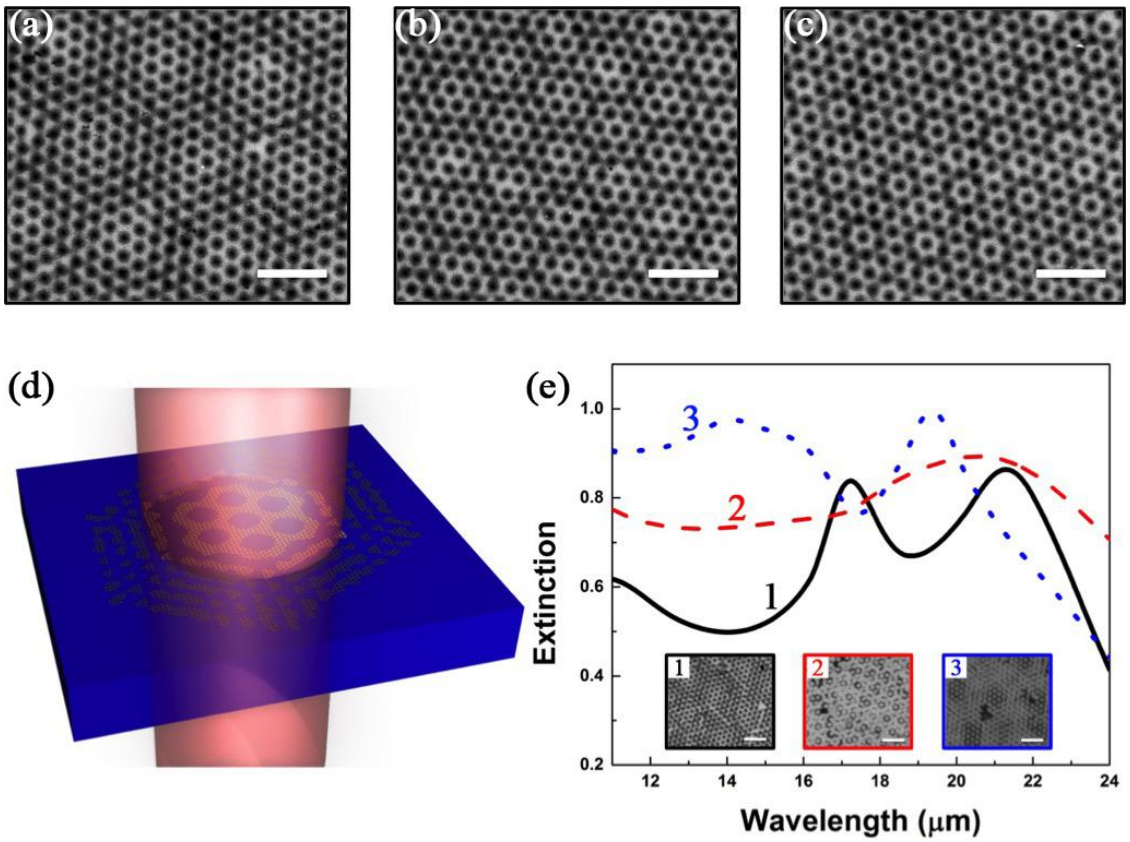

Figure 4.2 (a-c) SEM images of fabricated graphene moiré metasurfaces corresponding to relative rotation of (a) 7.5°, (b) 12°, and (c) 19°. (d) Schematic illustration of transmission extinction measurement of graphene moiré metasurfaces. The graphene nanostructures illuminated by incident light are excited to support surface plasmon resonances, resulting extinction in transmission. (e) Measured extinction spectra of three graphene moiré metasurfaces with different patterns. The black and white areas in SEM images are graphene and substrates, respectively. The scale bars are 1.5 μm. Reproduced here from [32]

GRAPHENE NANORIBBON PLASMONICS USING BLOCK COPOLYMER LITHOGRAPHY

Graphene nanoribbon (GNR) array displays strong light matter interactions through surface plasmons. GNR metasurface have been used for protein biosensing and mid-Infrared/terahertz spectroscopy [25-26]. The fabrication process of GNR array for plasmonic applications is often done using electron beam lithography (EBL) which cannot be scaled to large areas. Here we demonstrate for the first time fabrication of large area GNR array using block copolymer lithography (BCP). which takes advantage of the wetting transparency of graphene. Large area sub 20nm wide GNR array were successfully fabricated using this method. We performed Fourier transform infrared spectroscopy (FTIR) and Finite Element Method (FEM) simulation of our GNR array and could obtain strong broadband plasmon excitation peak at 1600cm^{-1}. This fabrication method can be used for wafer scale production of plasmonic modulators, sensors and photodetectors.

Fabrication of Large Area Graphene Nanoribbon Array

Fig 4.3 shows the schematic of our novel wetting transparency (WT) assisted large area GNR array fabrication process. Large area CVD grown monolayer graphene on Cu foil is transferred onto surface neutralized treatment (SNT) coated Si wafer by using PMMA assisted transfer method [5]. Graphene surface was treated with mild O_2 plasma to enhance its wettability to BCP solution. We spin coat PS-b-PMMA BCP solution on graphene. This sample is then annealed at 250C for 5mins to provide mobility for polymer to align into perpendicular lamellae. To use BCP as an etch mask for graphene, PMMA was selectively etch using CO_2 based etch process. The remaining PS acts an etch mask, and the pattern was etch transferred into underlying graphene to form GNR. After etching, the PS layer on top of the GNR is removed by soaking in THF for 12hrs. Fig 4.4a shows the SEM image of GNR array. The novelty of this process is that

GNR array is formed on top of SNT and does not require any additional steps to remove SNT layer. The GNR arrays can now be directly used for electrical and optical applications. This WT assisted BCP method can produce large area GNR array of different widths by choosing BCPs with different molecular weights.

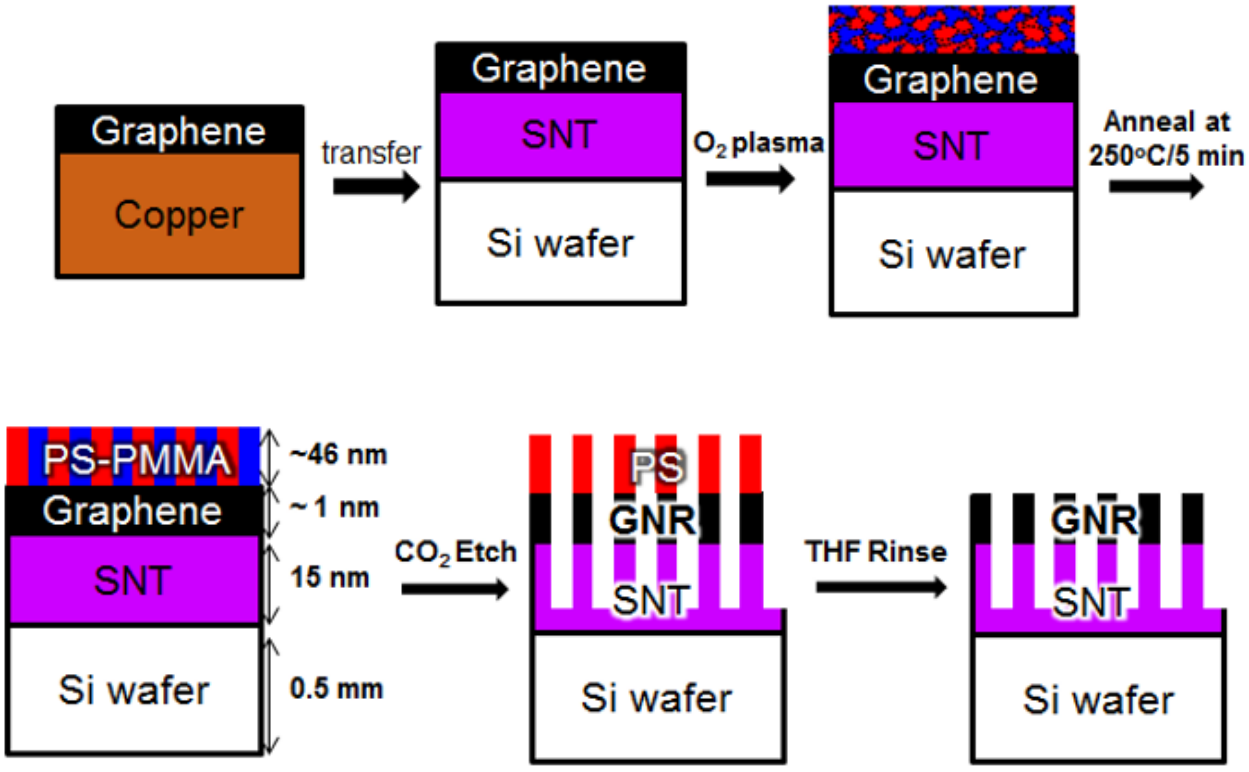

Figure 4.3: Schematic of our novel wetting transparency assisted large area GNR array fabrication process. Reproduced from [33]

FTIR Spectroscopy of GNR array

We performed FTIR spectroscopy of sub 20nm GNR array fabricated using WT assisted BCP method. We obtained strong broadband extinction peak at 1600 cm^{-1} as shown in fig 4.5(a). We designed GNR array for 1600cm^{-1} since it of very much interest

for protein bio sensing. We also studied tenability of plasmon resonance peak by simulating GNR of different widths (20nm to 60nm) as shown in Fig 4.5(b).

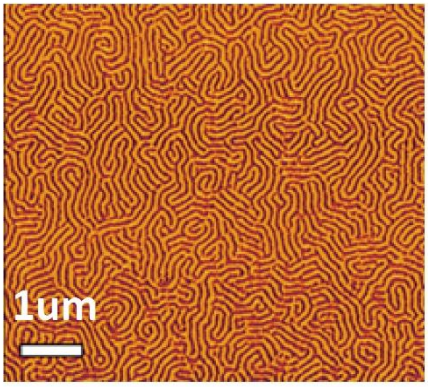

Figure 4.4: SEM image of GNR array

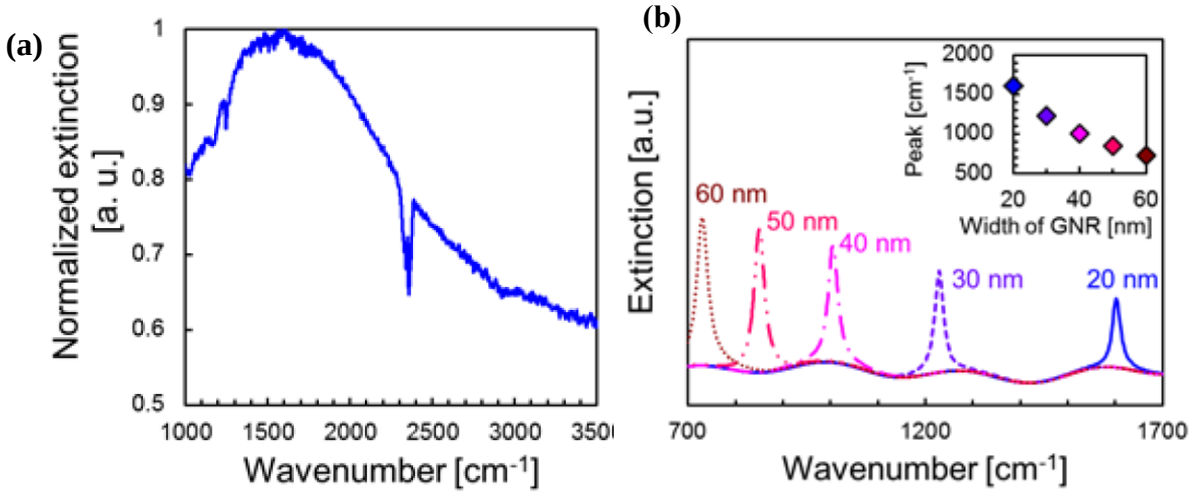

Figure 4.5: (a) Extinction spectra of GNR array. (b) Tenability for different widths

FEM analysis of GNR Metasurface

To corroborate the experimentally observed peak in the extinction spectrum and its relation to the graphene plasmons, we simulated the optical response of disordered arrays of graphene nanoribbons using Finite-element method simulation (FEM) software

COMSOL. Here, we picked a typical region of our sample with a large area $1\,\mu m \times 1\,\mu m$, and digitized the SEM image from that region (fig 4.6(a)) to determine the location of the GNRs on the surface. The obtained binary field then were fed into the FEM simulation as the graphene conductivity distribution. As can be seen from the simulation results in fig 4.6(b), the averaged optical extinction ratio shows a broad peak at 1600 cm^{-1}, which shows a good agreement with the experimental result (fig 4.5(a)). By studying the near field enhancement on the GNRs surface (fig 4.6(c)), we relate the peak in the spectrum to the excitation of graphene plasmons. Because of the disorder in the distribution of the GNRs size and location, two neighboring GNRs likely possess different resonance frequencies, resulting in the strong reflection of the graphene plasmons on the boundaries between two GNRs, creating high-Q factor localized plasmons, as indicated by the presence of hot spots on the near field distribution. We also emphasize that, due to the randomness in our system, the resonance frequencies of these localized graphene plasmons spans a large bandwidth, implying the presence of hotspots across the considered spectrum. Such bandwidth is very promising for sensing applications.

This work is done in collaboration with Prof. Christopher Elison (CHE Dept, UT Austin). I acknowledge Reika Katsumata, Stephen Sirard (LAM Research), Zilong Wu and Dr. Hossein Mousavi's contribution to this work.

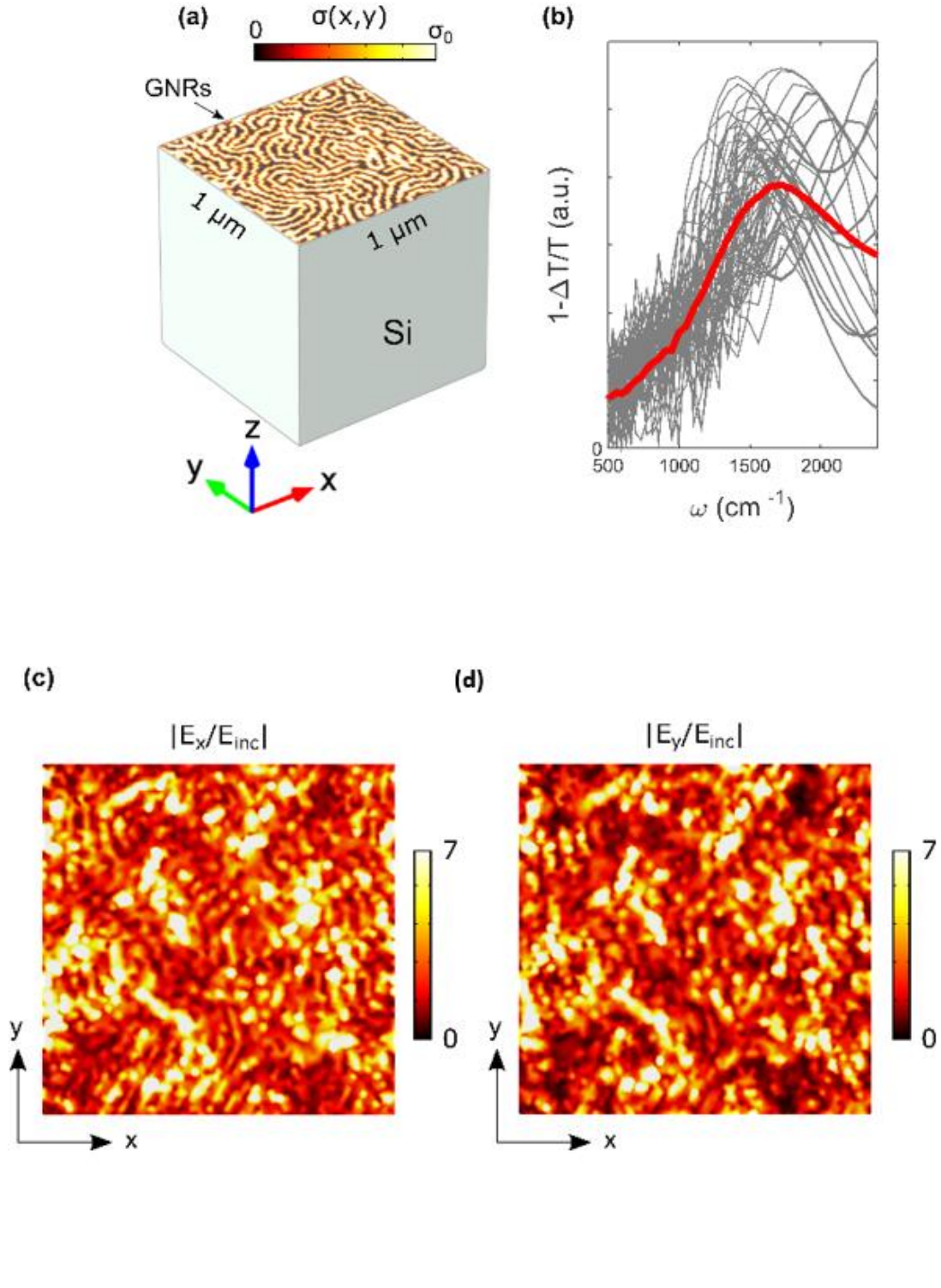
(a)
σ(x,y)
0
σ0
GNRs
1 μm
1 μm
Si
z
y
x
(b)
1-ΔT/T (a.u.)
0
500
1000
1500
2000
ω (cm -1)
(c)
|Ex/Einc|
7
0
y
x
(d)
|Ey/Einc|
7
0
y
x

Figure 4.6: FEM simulation of GNR array plasmon resonance. (a) Digitized SEM image of GNR. (b) averaged optical extinction ratio. (c), (d) near field enhancement on the GNRs surface.

PLASMONIC SCISSOR

Due to the high oxidation temperature of graphene, laser patterning of graphene requires high operation power. Ultrafast laser was used for direct patterning of graphene in the previous studies. Surface plasmons, which takes advantage of plasmon-enhanced photo thermal effect, i.e., the enhanced absorption of the metallic nanoparticles, we employ the continuous-wave (CW) laser to cut the graphene. Fig 4.7a shows the optical setup being used for laser based patterning of graphene. A thin layer of Au nanoparticles is deposited on the graphene for the patterning. We scan the focused laser beam on the sample using the spatial light modulator (SLM) or the computer-controlled motorized stage to create arbitrary patterns. Fig 4.7b shows the carton image of graphene on Au nano particle substrate used for patterning.

We fabricated various graphene patterns for mid-IR and terahertz plasmonics, which can be applied in plasmonic bio-sensing for detection of proteins or drugs [29]. Another direction is the design and fabrication of graphene metamaterials, which has attractive opportunities in terahertz detector and modulators.

We have some preliminary results of this patterning technique. Fig 4.8a. shows the large area graphene nanoribbons (2um) patterned using this method. Fig 4.8b shows the raman maping of the patterned graphene. The results are very promising for demonstration of mid- IR/THz plasmonics.

This work is done in collaboration with Prof. Yuebing Zheng's group (ME Dept, UT Austin). I acknowledge Dr. Linhan Lin and Wei Li's contribution to this ongoing work.

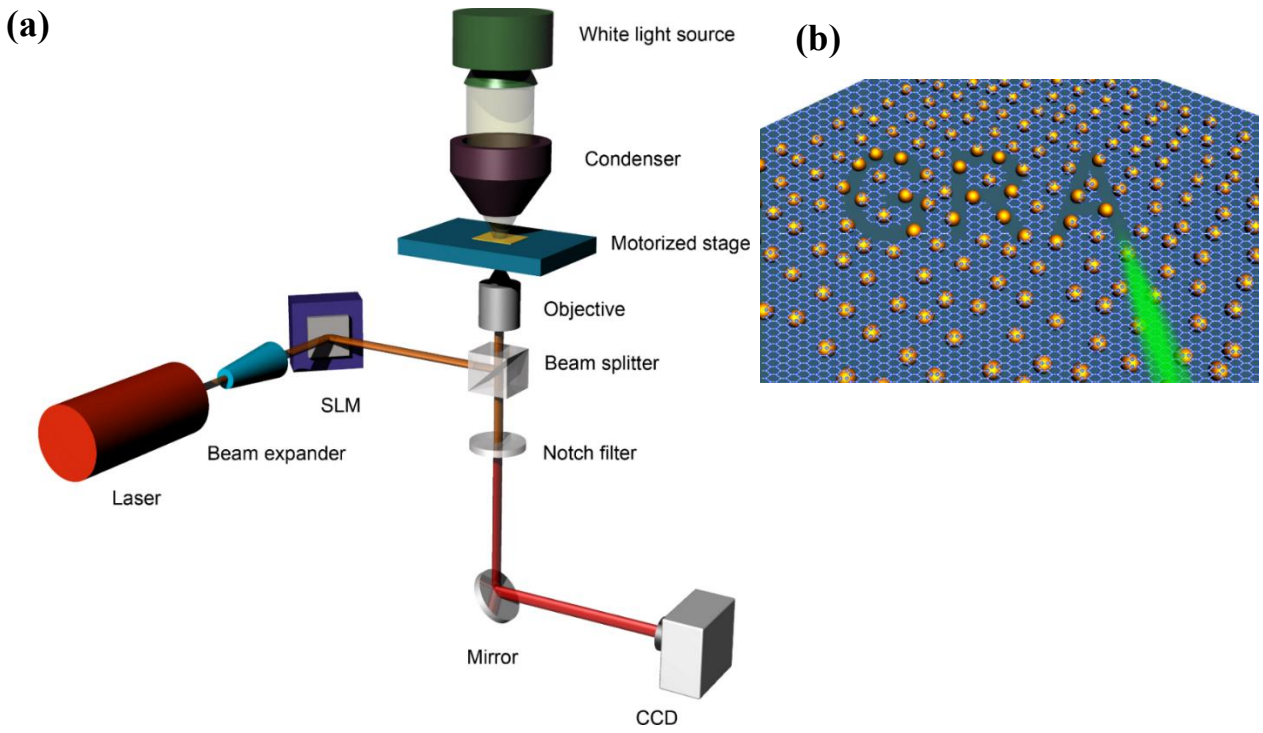

Figure 4.7: (a) Optical setup used for CW laser patterning. (b) Au nanoparticle coated graphene substrate.

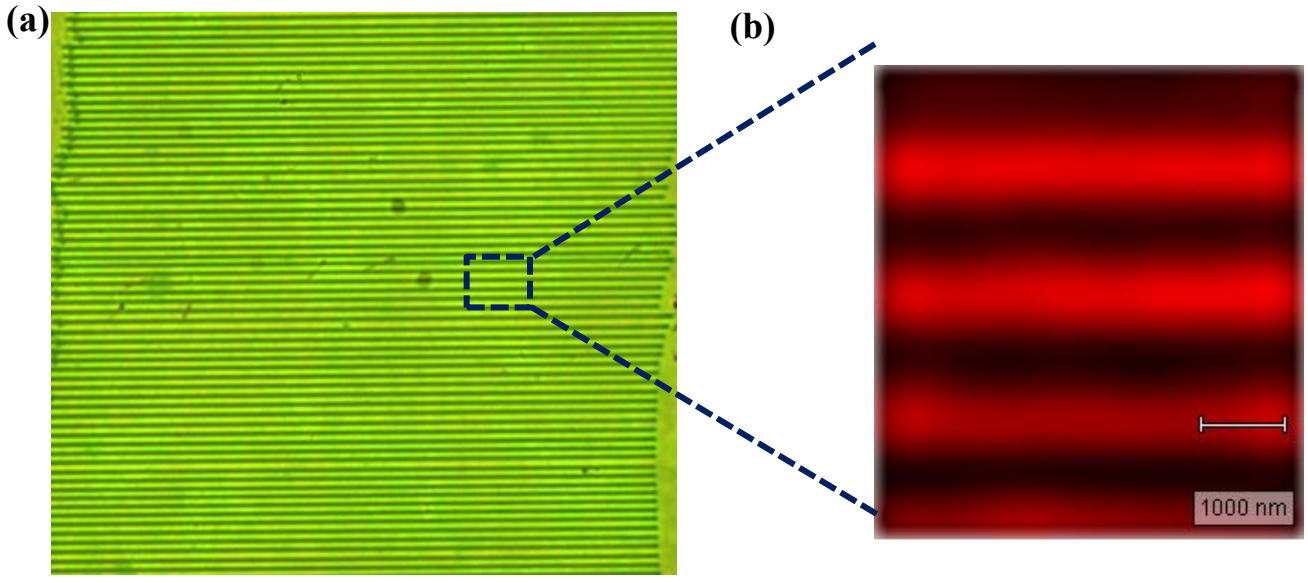

Figure 4.8: (a) Graphene nanoribbon patterned using CW laser technique. (b) Raman mapping of patterned graphene.

CONCLUSION

We introduced a cost-effective way to fabricate graphene moiré metasurfaces with high complexity and large gradient. Our results show that these metasurfaces are promising candidates for ultrathin plasmonic devices with tunable and multiband optical responses. The multiple plasmon resonance modes make graphene moiré metasurfaces promising candidates for ultrathin light modulators, biosensors, and photodetectors with multispectral responses.

We also successfully fabricated large area sub 20nm graphene nanoribbon array for plasmonic sensing application using novel WT assisted BCP method. We obtained strong broadband plasmon extinction peak at 1600cm-1 which was thoroughly analyzed by FEM simulation.

Chapter 5: MoS_2 based Plasmonics

PATTERNING MoS2 USING BUBBLE PEN LITHOGRAPHY

Lithography process normally involves using electrons, photons or chemical reactions to pattern two dimensional materials like MoS_2 or graphene [34-35] . This process normally takes long duration to complete. There is a need for a lithography tool which can pattern in real time two dimensional materials for different applications. Here, we have used novel bubble pen lithography (BPL) tool for real patterning two dimensional material (MoS_2).

BPL, a novel lithography tool designed by Dr. Linhan Lin (Prof. Yuebing Zheng's group, ME Dept, UT Austin) does arbitrary particle patterning using optically controlled microbubble.

High intensity laser beam generates a microbubble at the interface of plasmonic substrate and colloidal suspension via plasmon-enhanced photothermal effects. This microbubble captures colloidal particles (polysterene nanoparticles) on the substrate through actions of Marangoni convection, surface tension, gas pressure, and substrate adhesion. We can move this microbubble by moving the laser beam, and this can create different patterns.

Experimental

Fig 5.1a shows the experimental setup for BPL. We first transferred CVD monolayer MoS_2 onto glass substrate covered with 4nm gold nanoislands (AuNIs) using PMMA assisted wet transfer process [4] . Polysterene nanoparticle suspension is created on top of MoS_2 plasmonic substrate (MoS2/AuNI/Glass). We used 532 nm laser for generating microbubble at the interface between polysterene nanoparticle (960nm) suspension and MoS_2 plasmonic substrate. This microbubble is created due to plasmon

Note-This chapter results is published in the following journal – 1. Lin, et.al; Bubble-Pen Lithography. *Nano letters* **2016,** *16* (1), 701-8. I am coauthor on this journal and contributed significantly for many experimental results presented (device fabrication and measurements).

enhanced photothermal effect. This will introduce the Marangoni convection to collect polystyrene nanoparticles on the substrate (see Fig 5.1b). This particle gets trapped when force balance takes place [36]. It will be immobilized on the MoS_2 substrate by van der Waals interactions. Fig 5.1c shows the trapping process. Fig 5.1d, e shows the temperature and flow velocity distributions simulations. Fig 5.2 shows the CVD monolayer MoS_2 patterned by BPL. Interested readers are recommended to our work [37] for more details on BPL and its potential applications.

This work is done in collaboration with Prof. Yuebing Zheng's group (ME Dept, UT Austin). I acknowledge Dr. Linhan Lin and Wei Li's contribution to this work.

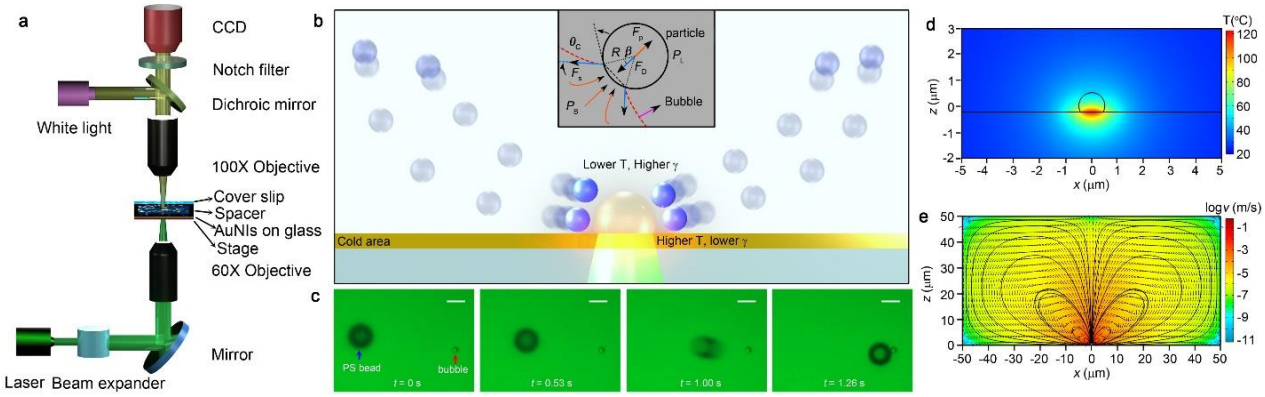

Figure 5.1: (a) Experimental setup for BPL. (b) Schematic illustration of the polystyrene nanoparticle trapping mechanism by microbubble. (c) Time-resolved trapping process of PS nanoparticle by a microbubble. (d) Simulated temperature distributions. (e) Simulated flow velocity distributions. Reproduced from [37]

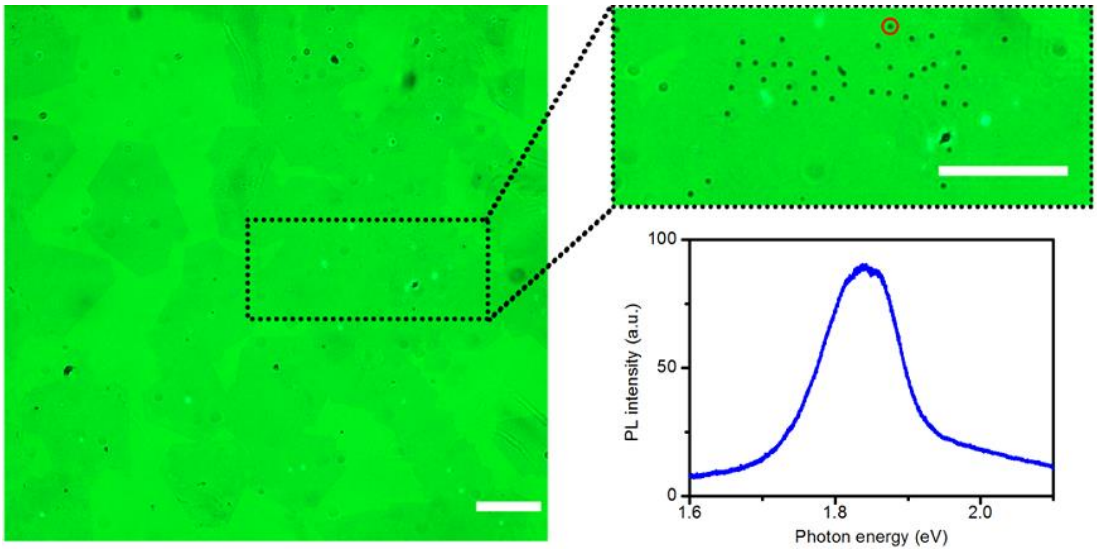

Figure 5.2: Optical micrographs of individual 960nm polystyrene beads patterned on the 2D monolayer CVD MoS_2 monolayer. Reproduced from [37]

ENHANCED LIGHT EMISSION FROM MoS_2 USING PNAS

Few layered MoS_2 has shown great promise for optics and electronics due to good mobility, band gap, atomic thickness, good electrostatic control, mechanical and thermal properties. Monolayer MoS_2 has a direct bandgap ~ 1.8eV. This makes it very interesting 2D material for photodetectors, LEDs and lasers [26]. Being monolayer limits its light absorption. Here, we present enhanced light emission from CVD monolayer MoS_2 using plasmonic nano antenna array (PNA) [38-39].

Experimental

PNA combines localized surface plasmon resonance of individual nanoantennas with lattice resonance. This leads to strong exciton – plasmon coupling in 2D materials like MoS_2. We simulated PNA for resonance at 1.8eV using Lumerical FDTD solver.

Fig 5.3a shows the schematic of PNAs on top of MoS_2. Monolayer MoS_2 is transferred onto quartz substrate using PMMA assisted transfer process (See section 3.2). EBL is used to pattern PNAs. We use Al for nanodiscs because of its resonance match with MoS_2 PL. We use thin spacer layer (PMMA) on top of the device to increase the Q factor of the plasmon resonace and decrease the dimension of nanodiscs. Fig 5.3b shows the SEM image of fabricated device. Inset shows the enlarged image of nanodiscs (~100nm). We have currently obtained ~ 2 times enhancement of PL. These results are very promising for future 2D nanomaterial based plasmonic LEDs.

This work is done in collaboration with Prof. Yuebing Zheng's group (ME Dept, UT Austin). I acknowledge Dr. Linhan Lin and Wei Li's contribution to this ongoing work.

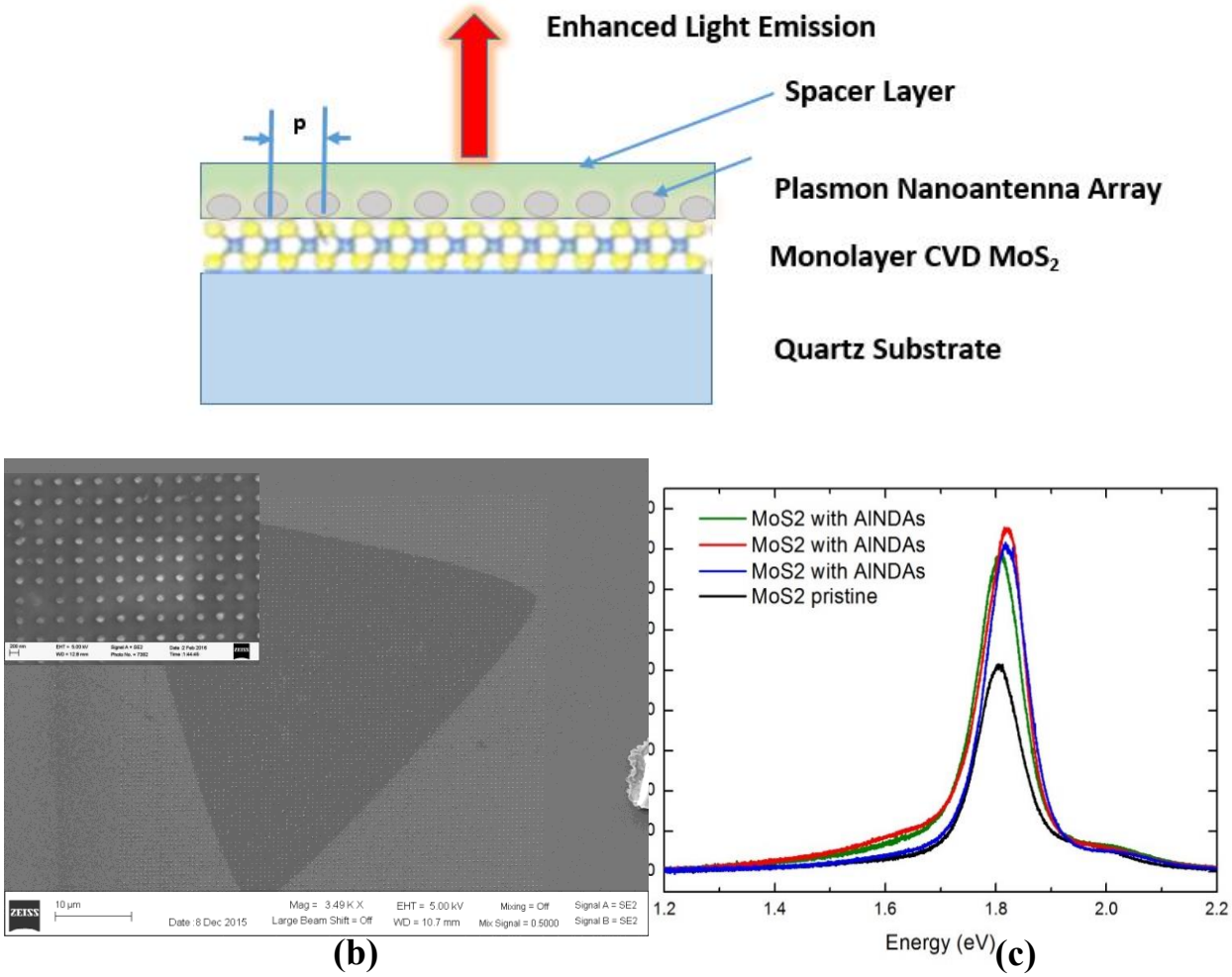

Figure 5.3: (a) Schematic of plasmonic nanoantenna array (PNA) on top of monolayer MoS_2. (b) SEM image of fabricated device. (c) MoS_2 photoluminescene enhancement with PNA.

CONCLUSION

In this work, we have shown novel method of real time patterning of large area CVD grown monolayer MoS_2 using bubble pen lithography. This process can be expanded towards roll to roll nanomanufacturing. We also showed light enhancement from monolayer MoS2 using plasmonic nanodisc array. This result is very promising for design of LEDs, lasers and photodetectors.

Chapter 6: Conclusion and Future Work

In this dissertation, we discussed graphene based flexible electronics in chapter 2. We demonstrated flexible CVD graphene based field effect RF transistors with record $f_T \sim$ 95GHz . We have also shown potential applications of those RF transistors for different circuits like demodulators and speakers. We have shown design of flexible antennas using multilayer graphene. All these results are very promising towards demonstration of all graphene based RF receiver. There are still many technical challenges to be overcome to demonstrate an all graphene based RF receiver. The important ones are, first, we should be able to grow very high quality large area graphene at low cost. Second, need to develop a good process flow to transfer this large area graphene onto flexible substrate and do real time roll to roll fabrication of transistors and passives circuit components. If these two problems are resolved then we can in future see graphene based RF receivers, sensors, displays and more.

MoS_2 based flexible electronics was discussed in chapter 3. MoS_2 having bandgap and good mobility, has good potential for low power digital/analog/RF circuits. We showed MoS_2 based flexible RF transistors operating n GHz range, and also demonstrated some useful RF circuits (amplifier, mixer and simple AM receiver) for IOT applications. In future, we can have all MoS_2 based flexible RF receiver for IOT application as shown in Fig 6.1. This receiver will be an integration of MoS_2 based low noise amplifier working at 1.2GHz, MoS_2 based RF mixer for down conversion and MoS_2 based baseband amplifiers. There are still many problems similar to graphene needs to be resolved to realize these receivers. Most important among them is the ability to synthesize wafer scale MoS2 and transfer it onto flexible substrate at low cost.

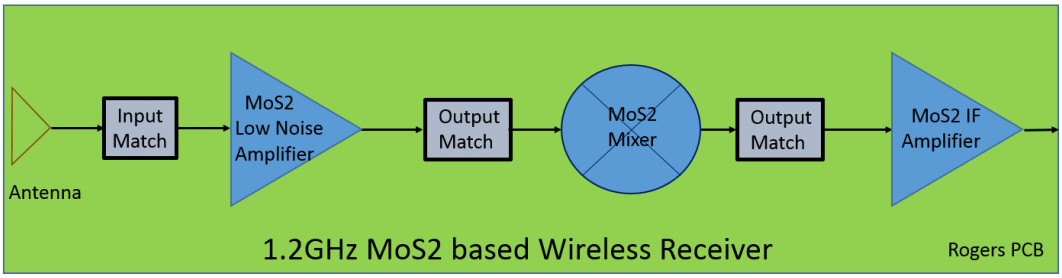

Figure 6.1: MoS2 based flexible Wireless Receiver

In chapter 4 and 5, we have shown design of novel plasmonic devices using 2D nanomaterials (graphene and MoS_2). We have demonstrated large area tunable graphene metasurface using moiré nanosphere lithography (MNSL). We have shown novel method to fabricate large area graphene nanoribbons (GNRs) using block copolymer lithography (BCPL) and its application towards tunable mid-IR plasmonic sensing. We report for the first time nanopatterning of CVD MoS_2 on plasmonic substrate using bubble pen lithography (BPL). We have also shown light enhancement of monolayer CVD MoS_2 using plasmonic nanoantenna array (PNA). These results are very useful for design of highly efficient 2D nanomaterial based LEDs, photodetectors, lasers and sensors.

Appendix A. De-embedding of RF transistors

S-parameter measurements were carried out on another flexible GFET device with G-S-G pads at gate and drain with source being the common ground. The measurement was done using Agilent VNA (E8361C) and cascade RF probe station. The intrinsic device data is obtained by employing a two-step de-embedding process. The device under test (GFET) can be modeled as shown in Fig A1. The intrinsic device data is obtained by employing a two-step de-embedding process. The Y-parameters of the device under test were obtained from extrinsic data, and afterwards the parasitics (obtained from open and short test structures) were de-embedded to determine the intrinsic device frequency response (see equation (A.1)). Y-parameter to S-parameter conversions are done using ADS circuit simulation tool.

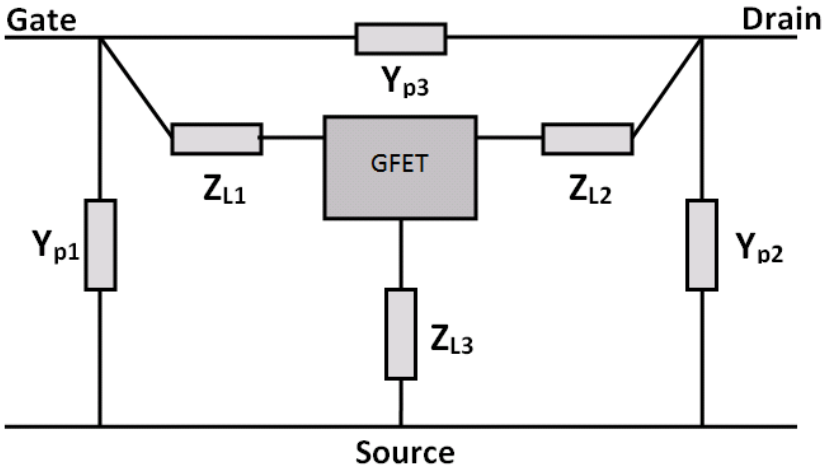

Figure A.1: RF model of GFET under test, where Y_{p1}, Y_{p2} and Y_{p3} are parallel parasitics and Z_{L1}, Z_{L2} and Z_{L3} are series parasitics (They represent GFET contact pads and interconnects). Reproduced from [8]

Note: This appendix results are published in the journal - *M. Yogeesh, et.al; Towards the Realization of Graphene Based Flexible Radio Frequency Receiver. Electronics* ***2015,*** *4*. I am first author and contributed for many experiments presented on this journal.

$$Y_{GFET} = ((Y\text{dut} - Y\text{open})^{-1} - (Y\text{short} - Y\text{open})^{-1})^{-1} \quad \text{----------A1}$$

Where Y_{GFET} is Y-parameters of intrinsic GFET, Ydut is Y-parameter of DUT (Extrinsic GFET), Yshort is the Y-parameter of DUT with gate, drain and source shorted, Yopen is DUT with no graphene channel. Here the graphene channel is etched by using reactive ion plasma etch tool. Yshort and Yopen will be deembeded from Ydut to get intrinsic GFET performance (YGFET).

Appendix B. MoS_2 Active Mixer Analysis

CVD MoS_2 FET gate input signal is given by:

$$v_g = A_{rf}\, cos(\omega_{rf}\, t) + A_{lo}\, cos(\omega_{lo}\, t)$$

…….....A3

Where A_{rf} and ω_{rf} correspond to the amplitude and frequency of the RF input signal. A_{lo} and ω_{lo} correspond to the amplitude and frequency of the LO input signal. We have neglected the gate bias V_g to simplify the small signal analysis.

The FET drain current is given by:

$$i_d = a_1 v_g + a_2 {v_g}^2 + higher\ order\ terms$$ …….....A4

Substituting Equation A3 in Equation A4 and expanding:

$$i_d = a_1(A_{rf}\, cos(\omega_{rf}\, t) + A_{lo}\, cos(\omega_{lo}\, t)) + a_2(A_{rf}\, cos(\omega_{rf}\, t) + A_{lo}\, cos(\omega_{lo}\, t))^2 +$$

$$higher\ order\ terms$$ ……A5

Expanding Equation A5:

$$i_d = a_1 A_{rf} \cos(\omega_{rf}\, t) + a_1 A_{lo} \cos(\omega_{lo}\, t)) + a_2 \frac{{A_{rf}}^2}{2}(1 + \cos(2\omega_{rf}\, t)) +$$

$$a_2 \frac{{A_{lo}}^2}{2}(1 + \cos(2\omega_{lo}\, t)) + a_2\,(\cos((\omega_{rf} - \omega_{lo})t) + a_2(\cos(\omega_{rf} + \omega_{lo})t) +$$

$$higher\ order\ terms$$…….A6

The drain current output of the mixer contains various intermodulation products (RF-LO, RF+LO, RF, LO, 2RF, 2LO). In Equation A6 the down converted signal is highlighted red and the up converted signal is green. Fig A.3 shows the spectrum of mixer output.

Note: This appendix results are published in the journal - Sanne, A.; et.al; Radio Frequency Transistors and Circuits Based on CVD MoS2. *Nano letters* **2015,** *15* (8), 5039-45; I am coauthor author and contributed for many experiments presented on this journal (simulations and measurements).

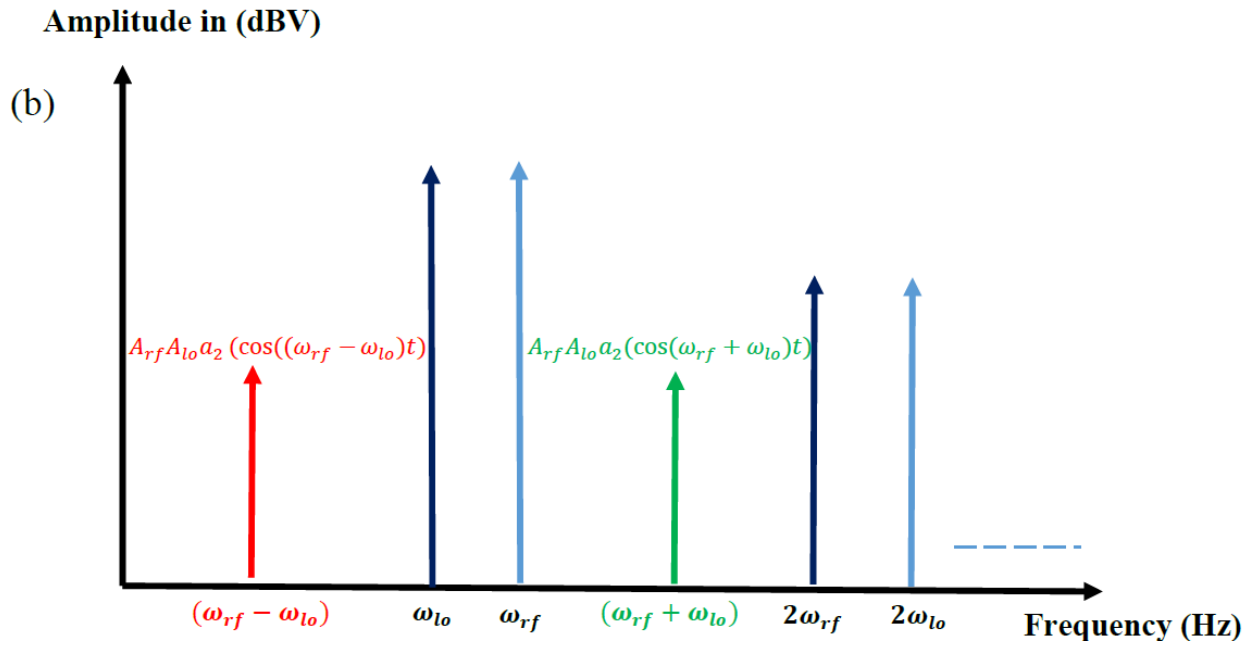

Figure B.1: Theoretical FFT spectrum of MoS_2 active mixer. Reproduced from [7]

References

1. Akinwande, D.; Petrone, N.; Hone, J., Two-dimensional flexible nanoelectronics. *Nature communications* **2014,** *5*, 5678.

2. Bae, S.; Kim, H.; Lee, Y.; Xu, X.; Park, J. S.; Zheng, Y.; Balakrishnan, J.; Lei, T.; Kim, H. R.; Song, Y. I.; Kim, Y. J.; Kim, K. S.; Ozyilmaz, B.; Ahn, J. H.; Hong, B. H.; Iijima, S., Roll-to-roll production of 30-inch graphene films for transparent electrodes. *Nature nanotechnology* **2010,** *5* (8), 574-8.

3. Chang, H. Y.; Yang, S.; Lee, J.; Tao, L.; Hwang, W. S.; Jena, D.; Lu, N.; Akinwande, D., High-performance, highly bendable MoS2 transistors with high-k dielectrics for flexible low-power systems. *ACS nano* **2013,** *7* (6), 5446-52.

4. Chang, H. Y.; Yogeesh, M. N.; Ghosh, R.; Rai, A.; Sanne, A.; Yang, S.; Lu, N.; Banerjee, S. K.; Akinwande, D., Large-Area Monolayer MoS2 for Flexible Low-Power RF Nanoelectronics in the GHz Regime. *Advanced materials* **2016,** *28* (9), 1818-23.

5. Lee, J.; Ha, T. J.; Li, H.; Parrish, K. N.; Holt, M.; Dodabalapur, A.; Ruoff, R. S.; Akinwande, D., 25 GHz embedded-gate graphene transistors with high-k dielectrics on extremely flexible plastic sheets. *ACS nano* **2013,** *7* (9), 7744-50.

6. Rahimi, S.; Tao, L.; Chowdhury, S. F.; Park, S.; Jouvray, A.; Buttress, S.; Rupesinghe, N.; Teo, K.; Akinwande, D., Toward 300 mm wafer-scalable high-performance polycrystalline chemical vapor deposited graphene transistors. *ACS nano* **2014,** *8* (10), 10471-9.

7. Sanne, A.; Ghosh, R.; Rai, A.; Yogeesh, M. N.; Shin, S. H.; Sharma, A.; Jarvis, K.; Mathew, L.; Rao, R.; Akinwande, D.; Banerjee, S., Radio Frequency Transistors and Circuits Based on CVD MoS2. *Nano letters* **2015,** *15* (8), 5039-45.

8. M. Yogeesh, K. N. P., J. Lee, S. Park, L. Tao, and D. Akinwande, Towards the Realization of Graphene Based Flexible Radio Frequency Receiver. *Electronics* **2015,** *4*.

9. Han, S. J.; Garcia, A. V.; Oida, S.; Jenkins, K. A.; Haensch, W., Graphene radio frequency receiver integrated circuit. *Nature communications* **2014,** *5*, 3086.

10. Lee, S.; Lee, K.; Liu, C. H.; Kulkarni, G. S.; Zhong, Z., Flexible and transparent all-graphene circuits for quaternary digital modulations. *Nature communications* **2012,** *3*, 1018.

11. Saungeun Park, S. H. S., Maruthi N. Yogeesh, Alvin L. Lee, Somayyeh Rahimi, and Deji Akinwande, Extremely High Frequency Flexible Graphene Thin Film Transistors. *IEEE Electron Device Letters* **2016**.

12. S Park, W. Z., HY Chang, MN Yogeesh, R Ghosh, SK Banerjee, D. Akinwande, High-frequency prospects of 2D nanomaterials for flexible nanoelectronics from baseband to sub-THz devices. *IEEE IEDM 2015* **2015**.

13. Maruthi Nagavalli Yogeesh, K. N. P., Deji Akinwande Flexible graphite antennas for plastic electronics. *IEEE ICEE 2014* **2014**.

14. Parrish, K., Nanoscale Graphene for RF Circuits and Systems. **2013**.

15. Maruthi Nagavalli Yogeesh, K. P., Jongho Lee, Li Tao, Deji Akinwande, Towards the design and fabrication of Graphene based flexible GHz radio receiver system. *IEEE IMS 2014* **2014**.

16. Li, X.; Cai, W.; An, J.; Kim, S.; Nah, J.; Yang, D.; Piner, R.; Velamakanni, A.; Jung, I.; Tutuc, E.; Banerjee, S. K.; Colombo, L.; Ruoff, R. S., Large-area synthesis of high-quality and uniform graphene films on copper foils. *Science* **2009,** *324* (5932), 1312-4.

17. Tian, H.; Ren, T. L.; Xie, D.; Wang, Y. F.; Zhou, C. J.; Feng, T. T.; Fu, D.; Yang, Y.; Peng, P. G.; Wang, L. G.; Liu, L. T., Graphene-on-paper sound source devices. *ACS nano* **2011,** *5* (6), 4878-85.

18. Wang, H.; Yu, L.; Lee, Y. H.; Shi, Y.; Hsu, A.; Chin, M. L.; Li, L. J.; Dubey, M.; Kong, J.; Palacios, T., Integrated circuits based on bilayer MoS(2) transistors. *Nano letters* **2012,** *12* (9), 4674-80.

19. Rai, A.; Valsaraj, A.; Movva, H. C.; Roy, A.; Ghosh, R.; Sonde, S.; Kang, S.; Chang, J.; Trivedi, T.; Dey, R.; Guchhait, S.; Larentis, S.; Register, L. F.; Tutuc, E.; Banerjee, S. K., Air Stable Doping and Intrinsic Mobility Enhancement in Monolayer Molybdenum Disulfide by Amorphous Titanium Suboxide Encapsulation. *Nano letters* **2015,** *15* (7), 4329-36.

20. A Sanne, M. N. Y., R Ghosh, A Rai, SH Shin, A Sharma, L Mathew, R Rao, D Akinwande, S Banerjee, Radio frequency transistors and circuit applications based on CVD MoS2. *IEEE Device Research Conference (DRC)* **2015**.

21. Atresh Sanne, S. P., Rudy Ghosh, Maruthi Nagavalli Yogeesh, Chison Liu, Leo Mathew, Rajesh Rao, Deji Akinwande, and Sanjay Banerjee, Embedded Gate CVD MoS2 Microwave FETs *Nature NPJ 2D Materials and Applications* **2017**.

22. Yeh, C. H.; Lain, Y. W.; Chiu, Y. C.; Liao, C. H.; Moyano, D. R.; Hsu, S. S.; Chiu, P. W., Gigahertz flexible graphene transistors for microwave integrated circuits. *ACS nano* **2014,** *8* (8), 7663-70.

23. Pozar, D. M., Microwave Engineering *Wiley Publication* **2008**.

24. Lili Yu, D. E.-D., Ujwal Radhakrishna, Xi Ling, Ahmad Zubair, Yuxuan Lin, Yuhao Zhang, Meng-Hsi Chuang, Yi-Hsien Lee, Dimitri Antoniadis, Jing Kong, Anantha Chandrakasan, and Tomas Palacios, Design, Modeling, and Fabrication of Chemical Vapor Deposition Grown MoS2 Circuits with E-Mode FETs for Large-Area Electronics. *Nano letters* **2016,** *16*.

25. Low, T.; Avouris, P., Graphene plasmonics for terahertz to mid-infrared applications. *ACS nano* **2014,** *8* (2), 1086-101.

26. Xia F, W. H., Xiao D, Dubey M, Ramasubramaniam A., Two-dimensional material nanophotonics. *Nat. Photonics* **2014**.

27. Yan H, L. X., Chandra B, Tulevski G, Wu Y, Freitag M, Zhu W, Avouris P, Xia F, Tunable infrared plasmonic devices using graphene/insulator stacks. *Nature nanotechnology* **2012**.

28. Marini A, S. I., García De Abajo FJ., Molecular Sensing with Tunable Graphene Plasmons. *ACS Photonics* **2015**.

29. Rodrigo, D.; Limaj, O.; Janner, D.; Etezadi, D.; Garcia de Abajo, F. J.; Pruneri, V.; Altug, H., APPLIED PHYSICS. Mid-infrared plasmonic biosensing with graphene. *Science* **2015,** *349* (6244), 165-8.

30. Chen, K.; Rajeeva, B. B.; Wu, Z.; Rukavina, M.; Dao, T. D.; Ishii, S.; Aono, M.; Nagao, T.; Zheng, Y., Moire Nanosphere Lithography. *ACS nano* **2015,** *9* (6), 6031-40.

31. Wu, Z.; Chen, K.; Menz, R.; Nagao, T.; Zheng, Y., Tunable multiband metasurfaces by moire nanosphere lithography. *Nanoscale* **2015,** *7* (48), 20391-6.

32. Zilong Wu, W. L., Maruthi Nagavalli Yogeesh, Seungyong Jung, Alvin Lynghi Lee, Kyle McNichola, Andrew Briggs, Seth Bank, Mikhail; Belkin, D. A., and Yuebing Zheng, Tunable and Gradient Graphene Metasurfaces by Self-assembly-based Moiré Nanosphere Lithography. *Adv Opt Mat* **2016**.

33. Reika Katsumata, M. N. Y., Helen Wong, Sunshine X Zhou, Stephen M Sirard, Tao Huang, Richard D Piner, Zilong Wu, Wei Li, Alvin L Lee, Matthew C Carlson, Michael J Maher, Deji Akinwande, Christopher J Ellison, Large area fabrication of graphene nanoribbons by wetting transparency-assisted block copolymer lithography. *Polymer* **2017,** *110*, 131-138.

34. Ito, T.; Okazaki, S., Pushing the limits of lithography. *Nature* **2000,** *406* (6799), 1027-31.

35. Rycenga, M.; Cobley, C. M.; Zeng, J.; Li, W.; Moran, C. H.; Zhang, Q.; Qin, D.; Xia, Y., Controlling the synthesis and assembly of silver nanostructures for plasmonic applications. *Chemical reviews* **2011,** *111* (6), 3669-712.

36. Zhao, C.; Xie, Y.; Mao, Z.; Zhao, Y.; Rufo, J.; Yang, S.; Guo, F.; Mai, J. D.; Huang, T. J., Theory and experiment on particle trapping and manipulation via optothermally generated bubbles. *Lab on a chip* **2014,** *14* (2), 384-91.

37. Lin, L.; Peng, X.; Mao, Z.; Li, W.; Yogeesh, M. N.; Rajeeva, B. B.; Perillo, E. P.; Dunn, A. K.; Akinwande, D.; Zheng, Y., Bubble-Pen Lithography. *Nano letters* **2016,** *16* (1), 701-8.

38. Lee, B.; Park, J.; Han, G. H.; Ee, H. S.; Naylor, C. H.; Liu, W.; Johnson, A. T.; Agarwal, R., Fano Resonance and Spectrally Modified Photoluminescence Enhancement in Monolayer MoS2 Integrated with Plasmonic Nanoantenna Array. *Nano letters* **2015,** *15* (5), 3646-53.

39. Liu, W.; Lee, B.; Naylor, C. H.; Ee, H. S.; Park, J.; Johnson, A. T.; Agarwal, R., Strong Exciton-Plasmon Coupling in MoS2 Coupled with Plasmonic Lattice. *Nano letters* **2016,** *16* (2), 1262-9.

40. Weinan zhu, Saungeun park, Maruthi Nagavalli Yogeesh and Deji Akinwande; Advancements in 2D Flexible Nanoelectronics: from material perspectives to RF applications.*Flexible and Printed Electronics*, IOP Science, Aug 2017

41. Sanne, Atresh, Saungeun Park, Rudresh Ghosh, Maruthi Nagavalli Yogeesh, Chison Liu, Leo Mathew, Rajesh Rao, Deji Akinwande, and Sanjay Kumar Banerjee. "Embedded Gate CVD MoS2 Microwave FETs." *npj 2d materials and applications* 1, no. 1 (2017): 26.